

1 **Insights into characteristics and formation mechanisms of secondary organic**  
2 **aerosols in Guangzhou urban area**

3 **Miaomiao Zhai<sup>1,3</sup>, Ye Kuang<sup>1,3\*</sup>, Li Liu<sup>2,\*</sup>, Yao He<sup>1,3</sup>, Biao Luo<sup>1,3</sup>, Wanyun Xu<sup>4</sup>, Jiangchuan**  
4 **Tao<sup>1,3</sup>, Yu Zou<sup>2</sup>, Fei Li<sup>2,5</sup>, Changqin Yin<sup>2,7</sup>, Chunhui Li<sup>2</sup>, Hanbing Xu<sup>6</sup>, Xuejiao Deng<sup>2</sup>**

5 <sup>1</sup> Institute for Environmental and Climate Research, Jinan University, Guangzhou, China.

6 <sup>2</sup> Key Laboratory of Regional Numerical Weather Prediction, Institute of Tropical and Marine  
7 Meteorology, China Meteorological Administration, Guangzhou, 510640, China

8 <sup>3</sup> Guangdong-Hongkong-Macau Joint Laboratory of Collaborative Innovation for Environmental  
9 Quality, Guangzhou, China.

10 <sup>4</sup> State Key Laboratory of Severe Weather & Key Laboratory for Atmospheric Chemistry, Institute of  
11 Atmospheric Composition, Chinese Academy of Meteorological Sciences, Beijing, 100081, China

12 <sup>5</sup> Xiamen Key Laboratory of Straits Meteorology, Xiamen Meteorological Bureau, Xiamen, 361012,  
13 China

14 <sup>6</sup> Experimental Teaching Center, Sun Yat-Sen University, Guangzhou 510275, China

15 <sup>7</sup> Shanghai Key Laboratory of Meteorology and Health, Shanghai Meteorological Bureau, Shanghai  
16 200030, China

17 \*Correspondence to: Ye Kuang (kuangye@jnu.edu.cn) and Li Liu (liul@gd121.cn)

18  
19  
20  
21  
22  
23  
24  
25  
26  
27  
28  
29  
30  
31  
32  
33  
34  
35  
36  
37

38 **Abstract**

39 Emission controls have substantially brought down aerosol pollution in China, however, aerosol  
40 mass reductions have slowed down in recent years in the Pearl River Delta (PRD) region, where  
41 secondary organic aerosol (SOA) formation poses a major challenge for air quality improvement. In  
42 this study, we characterized the roles of SOA in haze formation in urban Guangzhou City of the PRD  
43 using year-long aerosol mass spectrometer measurements for the first time and discussed possible  
44 pathways of SOA formations. On average, organic aerosols (OA) contribute dominantly (50%) to non-  
45 refractory submicron aerosol mass (NR-PM<sub>1</sub>). The average mass concentration of SOA (including by  
46 less and more oxidized OA, LOOA and MOOA) contributed most to NR-PM<sub>1</sub>, reaching about 1.7  
47 times that of primary organic aerosols (POA, including hydrocarbon-like and cooking-related OA) and  
48 accounting for 32% of NR-PM<sub>1</sub>, even more than sulfate (22%) and nitrate (16%). Seasonal variations  
49 of NR-PM<sub>1</sub> revealed that haze formation mechanisms differed much among distinct seasons. Sulfate  
50 mattered more than nitrate in fall, while nitrate was more important than sulfate in spring and winter,  
51 with SOA contributing significantly to haze formations in all seasons. Daytime SOA formation was  
52 weak in winter under low oxidant level and air relative humidity, whereas prominent daytime SOA  
53 formation was observed in fall, spring and summer almost on a daily basis, suggesting important  
54 roles of photochemistry in SOA formations. Further analysis showed that the coordination of gas-phase  
55 photochemistry and subsequent aqueous-phase reactions likely played significant roles in quick  
56 daytime SOA formations. Obvious nighttime SOA formations were also frequently observed in spring,  
57 fall and winter, and it was found that daytime and nighttime SOA formations together had resulted in  
58 the highest SOA concentrations in these seasons and contributed substantially to severe haze  
59 formations. Simultaneous increases of nitrate with SOA after sunset suggested the important roles of  
60 NO<sub>3</sub> radical chemistry in nighttime SOA formations, and this was further confirmed by continuous  
61 increase of NO<sup>+</sup>/NO<sub>2</sub><sup>+</sup> fragment ratio that related to measured particulate nitrate after sunset. Findings  
62 of this study have promoted our understanding of haze pollution characteristics of the PRD and laid  
63 down future directions on investigations of SOA formation mechanisms in urban areas of southern  
64 China that share similar emission sources and meteorological conditions.

65

## 66 **1 Introduction**

67 Ubiquitous submicron aerosols in the atmosphere not only deteriorate human health and visibility,  
68 but also impact climate through interactions with solar radiation and clouds. Organic aerosols (OA)  
69 represent one of the most important and sometimes even dominant components (~10-90%) of PM<sub>1</sub>  
70 (aerosol particles with aerodynamic diameter less than 1 μm) in urban, rural and remote areas (Zhang  
71 et al., 2007; Jimenez et al., 2009). OA can either be emitted directly from emission sources or be formed  
72 through atmospheric reactions of volatile organic compounds, the former is referred to as primary OA  
73 (POA) and the latter is referred to as secondary OA (SOA). An increasing number of studies show that  
74 SOA account for a large fraction of OA worldwide (Zhang et al., 2007; Zhang et al., 2011), and even  
75 dominate in some cases (Kuang et al., 2020). The implementation of strict emission reduction policies  
76 has significantly improved the air quality of Pearl River Delta (PRD) region, which is a highly  
77 industrialized area of China, and the annual mean concentration of PM<sub>2.5</sub> (particulate matter with  
78 aerodynamic diameter less than 2.5 μm) has been brought down to less than 30 μg/m<sup>3</sup> (Xu et al., 2020).  
79 However, the reduction of PM<sub>2.5</sub> mass concentrations in PRD has slowed down substantially in recent  
80 years, which might be related to the significant increases in the proportion of secondary aerosols (Xu  
81 et al., 2020), especially for SOA. Insights into SOA formation mechanisms are important for air  
82 pollution improvement.

83 SOA formation mechanisms are an active research area of interest in atmospheric chemistry in the  
84 recent ten years since significant contributions of SOA to atmospheric aerosol mass have been  
85 recognized (Zhang et al., 2007; Jimenez et al., 2009), however quite complex due to varying precursors,  
86 oxidants and formation pathways under different emission characteristics and meteorological  
87 conditions. As to SOA formation pathways, SOA can be formed through condensation of oxidized gas-  
88 phase organic vapors during the oxidation of volatile organic compounds (VOCs), this type of formed  
89 SOA was usually referred to as gasSOA (Kuang et al., 2020). SOA can also be formed in the aqueous  
90 phase through the further oxidation of dissolved VOCs which are usually products of gas-phase  
91 oxidation of VOCs, this type of SOA was usually referred as aqSOA (Ervens et al., 2011). Both field  
92 measurements and laboratory studies are needed in investigating detailed SOA formation mechanisms  
93 in different regions. Field measurements provide insights into key oxidants and formation pathways  
94 under ambient conditions, thus information from field measurements are important for both designing

95 laboratory experiments and targeting emission control strategies. Aerosol mass spectrometers are  
96 advanced on-line instruments that provide real time quantitative characterization of aerosol particle  
97 compositions (Jayne et al., 2000;Canagaratna et al., 2007;Jimenez et al., 2003). Positive matrix  
98 factorization (PMF) (Ulbrich et al., 2009) or a multilinear engine (ME-2) (Paatero, 1999;Canonaco et  
99 al., 2013) can be employed to further resolve different OA factors that are associated with different  
100 sources and formation mechanisms from the OA mass spectra. Using these techniques, the SOA  
101 sources and formation mechanisms are extensively investigated in China (Zhou et al., 2020), and many  
102 studies found that aqueous reactions in aerosol water contributed substantially even dominantly to  
103 SOA formations (Su et al., 2020) in haze episodes with daytime and nighttime SOA formations differ  
104 much due to different meteorological conditions and oxidants (Rollins et al., 2012;Huang et al., 2021).

105 In fact, in a specific region, the compositions, sources, and evolution processes differ much among  
106 seasons due to changes in emission sources and meteorological conditions (Li et al., 2015). Therefore,  
107 long-term observations that cover measurements of different seasons were usually needed for  
108 characterizing OA sources and SOA formation mechanisms, thereby helping to address the challenge  
109 of fine particulate matter pollution mitigation. Even though aerosol mass spectrometers have been  
110 widely used in China in recent years, most studies have been conducted in specific periods due to its  
111 high cost and maintenance (He et al., 2011;Chen et al., 2021b;Qin et al., 2017), resulting in few long-  
112 term characterizations of the mass concentrations and chemical compositions of submicron particulate  
113 matter (PM<sub>1</sub>). The design of Aerosol Chemical Speciation Monitor (ACSM) has improved this problem  
114 to some extent (Ng et al., 2011;Sun et al., 2015;Canonaco et al., 2021). For example, based on 2-year  
115 ACSM measurements, Sun et al. (2018) investigate the distinct characteristics of PM<sub>1</sub> compositions  
116 among different seasons in Beijing urban area and illustrated the dominant role of SOA in OA across  
117 different mass loading scenarios during all seasons.

118 Guangzhou is an expansive metropolis in the highly industrialized PRD region. Using the aerosol  
119 mass spectrometer measurements and source apportionment technique, Qin et al. (2017) and Huang et  
120 al. (2011) reported that SOA contributed substantially to aerosol mass during autumn and winter in  
121 Guangzhou. Guo et al. (2020) found that OA played a dominant role in PM<sub>1</sub> during winter in  
122 Guangzhou, with OA source apportionment emphasized the dominance of SOA. Guo et al. (2020) also  
123 suggested that gasSOA contributed predominantly to SOA formation during non-pollution periods,

124 other mechanisms such as heterogeneous and multiphase reactions played more important roles in  
125 SOA formation during pollution episodes, however long-term aerosol spectrometer measurements that  
126 help characterizing OA sources and SOA formation mechanisms in this region remain lacking. In this  
127 study, we performed a year-long continuous measurement of non-refractory submicron aerosols (NR-  
128 PM<sub>1</sub>) with an ACSM in urban Guangzhou from September 2020 to August 2021 to characterize POA  
129 sources and investigate SOA formation mechanisms in different seasons.

## 130 **2 Experimental methods**

### 131 **2.1 sampling site and measurements**

132 A quadrupole-Aerosol Chemical Speciation Monitor (Q-ACSM) was deployed to continuously  
133 measure nonrefractory PM<sub>1</sub> (NR-PM<sub>1</sub>) species including OA, sulfate (SO<sub>4</sub>), nitrate (NO<sub>3</sub>), ammonium  
134 (NH<sub>4</sub>), and chloride (Cl) from September 2020 to August 2021 at an urban site located in Haizhu  
135 wetland park of Guangzhou, which is surrounded by commercial streets and residential buildings,  
136 however, with a distance of at least 1 km (Liu et al., 2022). Therefore, measurements at this site are  
137 representative of the pollution characteristics of Guangzhou urban area. More detailed descriptions  
138 about the sampling site and the ACSM measurements could be referred to Liu et al. (2022) and Ng et  
139 al. (2011), respectively. An AE33 aethalometer (Drinovec et al., 2015) set up with a flow rate of 5  
140 L/min was separately operated downstream of a PM<sub>2.5</sub> inlet (BGI SCC 1.829) to measure aerosol  
141 absorptions, from which optically equivalent black carbon (BC) mass concentrations in winter and  
142 early spring were calculated. In addition, mass concentrations of PM<sub>2.5</sub> and trace gases such as nitrogen  
143 dioxide (NO<sub>2</sub>), ozone (O<sub>3</sub>), carbon monoxide (CO) and sulfur dioxide (SO<sub>2</sub>) were acquired from the  
144 publicly available datasets of the China National Environmental Monitoring network  
145 (<http://www.cnemc.cn/en/>), which includes a site located within 5 km distance to our observation site.  
146 Measurements of meteorological parameters such as temperature, wind speed and direction (WS and  
147 WD), and relative humidity (RH) were made by an automatic weather station (Li et al., 2021). Aerosol  
148 liquid water content (ALWC) was predicted with the ISORROPIA-II thermodynamic model in reverse  
149 mode under metastable assumption (Guo et al., 2017) with aerosol chemical compositions measured  
150 by Q-ACSM as inputs, with more details in Supplement Sect.S2.

## 151 2.2 Q-ACSM data analysis

152 The Q-ACSM data were processed using ACSM standard data analysis software (ACSM Local  
153 1.5.10.0 Released July 6, 2015) written in Igor Pro (version 6.37). The composition-dependent  
154 collection efficiency (CE) parameterization scheme proposed by Middlebrook et al. (2012) was chosen  
155 to determine the mass concentrations of NR-PM<sub>1</sub> species which was also detailed in Liu et al. (2022).  
156 Relative ionization efficiencies (RIEs) of 5.15 and 0.7 were adopted for ammonium and sulfate  
157 quantifications which were calibrated using 300 nm pure NH<sub>4</sub>NO<sub>3</sub> and (NH<sub>4</sub>)<sub>2</sub>SO<sub>4</sub> while the default  
158 RIEs of 1.4, 1.1 and 1.3 was used for organic aerosol, nitrate and chloride, respectively. Moreover, we  
159 also compared the mass concentrations of NR-PM<sub>1</sub> with PM<sub>2.5</sub> to ensure the validity of ACSM data  
160 during the whole study. As shown in Fig. S1 of the supplement, the measured NR-PM<sub>1</sub> correlates  
161 highly with PM<sub>2.5</sub> acquired from the nearest (about 5 km) Environmental Protection Agency site ( $R^2 =$   
162 0.71), and the average ratio of NR-PM<sub>1</sub>/PM<sub>2.5</sub> is 0.77 ( $\pm 0.36$ ).

163 Unconstrained Positive matrix factorization (PMF) was performed on OA mass spectra of the  
164 entire year-long dataset. For the two-factor solution, the POA factor peaking in the evening with low  
165 O/C ( $\sim 0.28$ ) and an oxygenated OA (OOA) factor peaks in the afternoon with high O/C ( $\sim 0.88$ ) can  
166 be well resolved (Fig.S2), demonstrating the markedly different influences of primary emissions and  
167 SOA formations on diel aerosol mass concentrations. However, PMF-ACSM analysis of mass spectra  
168 of OA measured by unit mass resolution instruments still faced some uncertainties to further resolve  
169 potential POA or SOA components due to its rotational indeterminacy. For example, traffic-related  
170 hydrocarbon-like organic aerosols (HOA) was sometimes not well separated from cooking-related  
171 organic aerosols (COA) and there was also great uncertainty in distinguishing SOA with different  
172 degrees of oxidations (Sun et al., 2012; Sun et al., 2013; Zhang et al., 2015). Therefore, an improved  
173 source apportionment technique called Multilinear Engine (ME-2) was further used to resolve better  
174 sources of POA and SOA (Paatero, 1999; Canonaco et al., 2013; Guo et al., 2020). Previously, both Guo  
175 et al. (2020) and Liu et al. (2022) demonstrated that during both autumn and winter seasons of  
176 Guangzhou urban areas, POA was mainly composed of HOA (which is mostly associated with traffic  
177 emissions) and COA, while SOA could be resolved into less oxidized and more oxidized organic

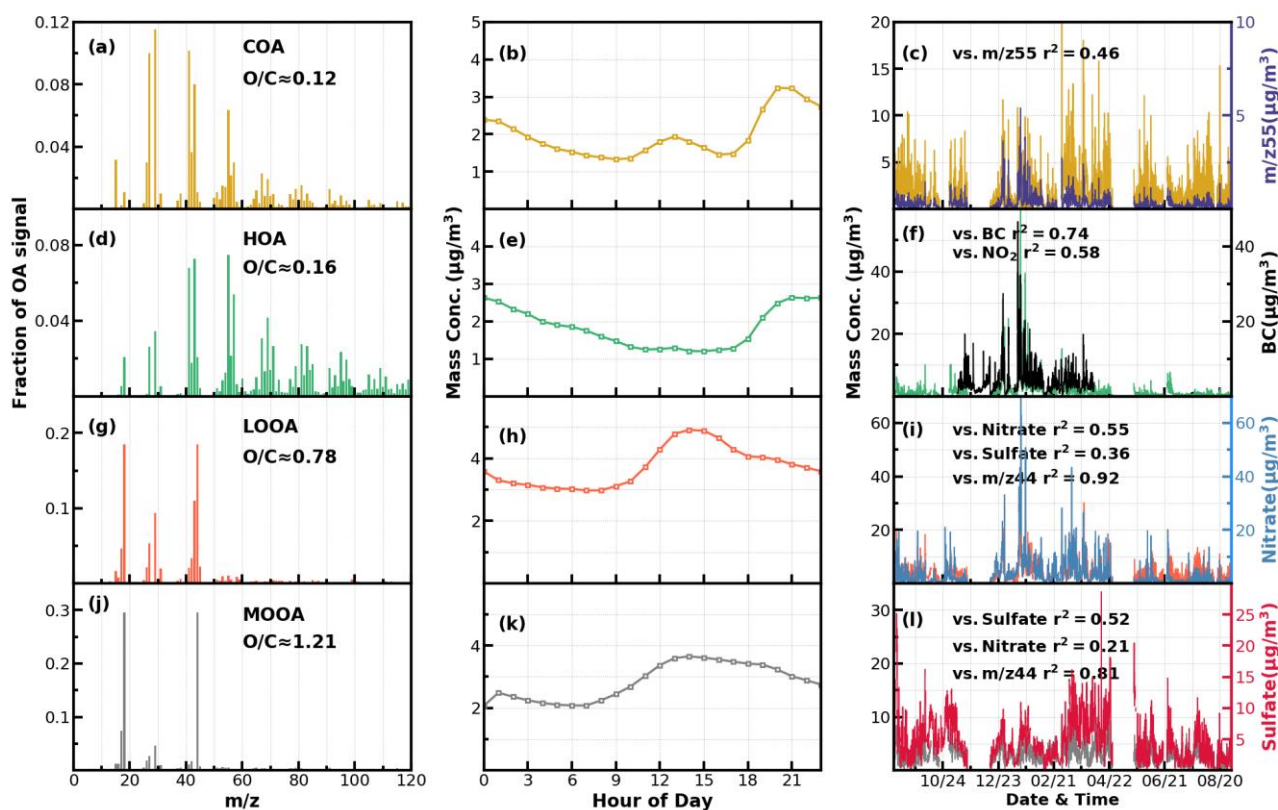


**Figure 1.** Mass spectral profiles, diurnal cycles and correlations with external data of COA(a-c), HOA(d-f), LOOA(g-i) and MOOA(j-l) from ME2-ACSM analysis for the entire year.

178 aerosols (LOOA and MOOA). The number selecting test using unconstrained PMF analysis (Fig.S3)  
 179 also showed that four-factor solution likely be the best choice. Therefore, we had chosen 4 factors for  
 180 ME-2 analysis with the  $a$  value of ME-2 ranging from 0.1 to 0.5. Furthermore we constrained the  
 181 HOA and COA profiles with HOA and COA profiles reported in Liu et al. (2022) as priories  
 182 considering the following three reasons: (1) The used instrument of this study is the same one of Liu  
 183 et al. (2022); (2) the COA profile reported in Liu et al. (2022) was determined during the period when  
 184 both COVID-19 silence-action and festival spring occurred when cooking activities grew and traffic  
 185 activities almost vanished thus COA shall dominated over HOA; (3) Resolved variations of HOA and  
 186 COA are well explained by external datasets. For example, correlations of HOA with black carbon  
 187 reached 0.79. The four-factor solution using the ME-2 technique with  $a=0.2$  was obtained and shown  
 188 in Fig.1. The resolved HOA and COA are summed as POA, resolved LOOA and MOOA are summed  
 189 as SOA, and the comparison with those resolved by the PMF is shown in Fig.2. ME-2 analysis  
 190 generally reproduced both the diurnal variations as well as absolute mass concentrations of POA and  
 191 SOA during different months well. To explore the consistency of resolved factors using the entire year-

192 long dataset or only using seasonal dataset when performing ME-2 analysis, we performed individual  
 193 ME-2 runs for each season. Results showed that factors resolved in each season using seasonal datasets  
 194 as inputs of ME-2 are generally consistent with those resolved from year-long dataset (Fig.S4-S7).  
 195 Therefore, factors resolved using the entire year-long dataset as input of ME-2 were used for further  
 196 investigations and this also guaranteed consistency of factors for comparisons among seasons.

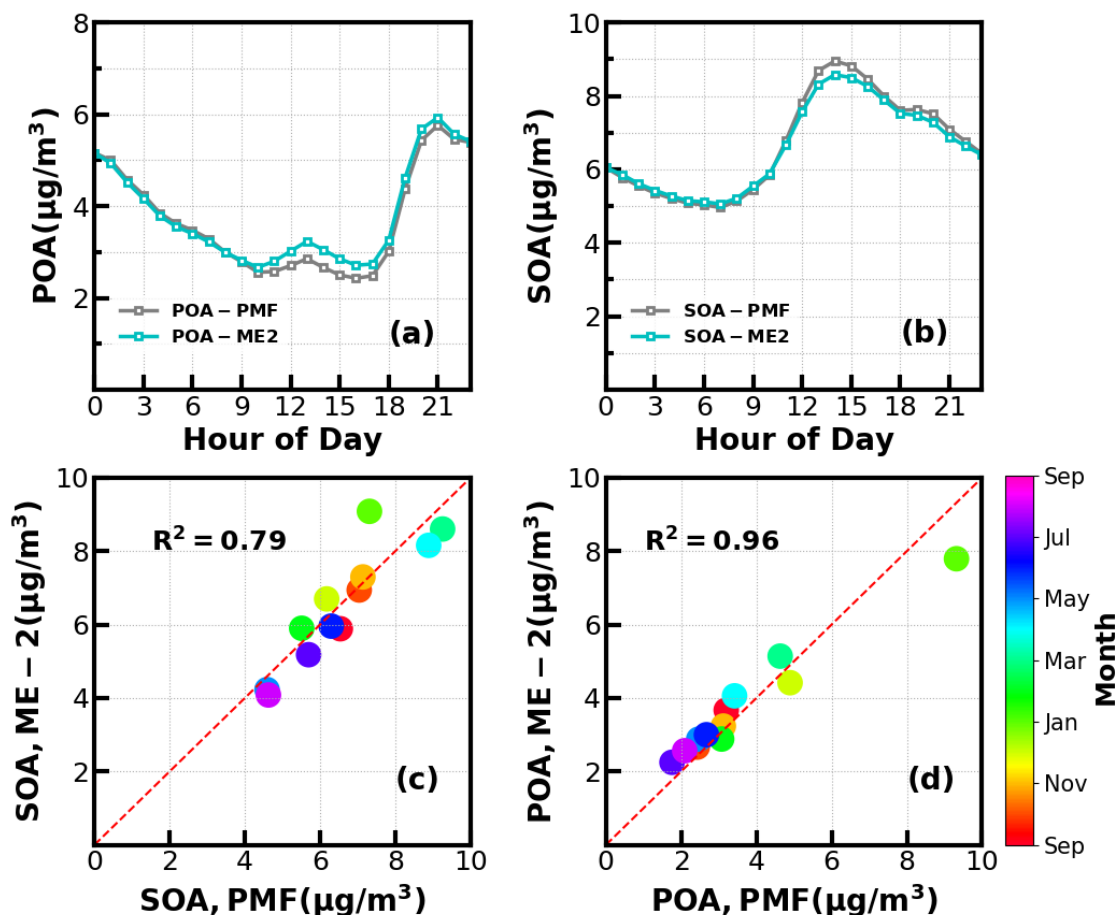


**Figure 2.** (a) and (b) Diurnal variations of POA and SOA concentrations from ME-2 and PMF; (c) and (d) Scatter plots between monthly average POA and SOA concentrations from ME-2 and PMF.

197 The mass spectrum of COA deconvolved in this work was characterized by a high  $m/z$  55-to-57  
 198 ratio of 2.12, which was the same with the one reported by Guo et al. (2020), and close to the  $m/z$  55-  
 199 to-57 ratio range of 2.2-2.8 reported by Mohr et al. (2012) for COA. Similar to previous studies (Guo  
 200 et al., 2020; Sun et al., 2013), the concentration of COA was well correlated ( $R^2=0.46$ ) with  $m/z$  55.  
 201 The O/C ratio of 0.12 for COA revealed that it was less oxidized than HOA (O/C=0.16) during the  
 202 whole year in Guangzhou, which was contrary to Sun et al. (2011). As shown in Fig.3, the diurnal  
 203 profile of COA presented two typical peaks during the entire year with a noontime peak during 13:00  
 204 - 14:00 LT and an evening peak during 20:00 - 21:00 LT, which were associated with noon and evening



205 cooking activities. It was noteworthy that the nighttime peak concentration of COA was very close to  
 206 that of noontime in summer, while the evening peak of COA was significantly higher than that of  
 207 noontime in other three seasons. The ratio of evening COA peak to that of the noontime was 1.7 in fall,  
 208 and was 1.6 in spring. In particular, the evening COA peak was nearly 4 times that of noontime in  
 209 winter due to the relatively insignificant noontime peak during this period, which might be associated  
 210 with the lock down and spring festival in winter which resulted in less noontime activities. Similar

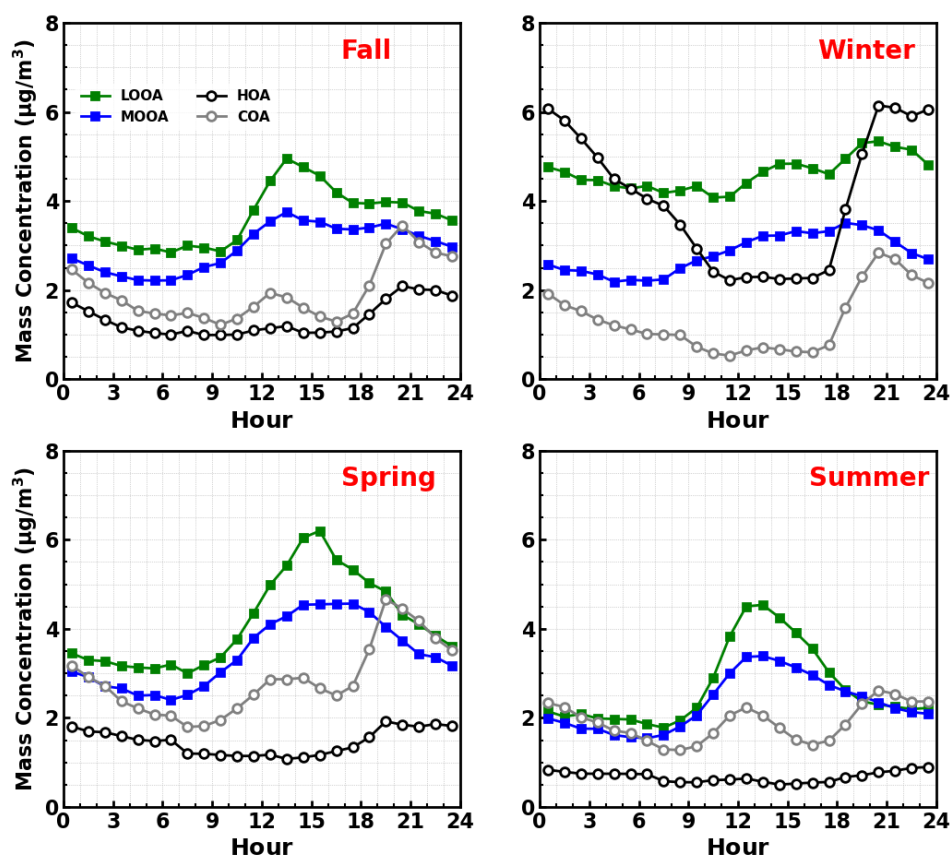


**Figure 3.** Diurnal profiles of HOA, COA, LOOA and MOOA in spring (March to May), summer (June to August), Fall (September to November), Winter (December to February).

211 conclusions could be found in Sun et al. (2018). More frequent cooking activities at night such as the  
 212 Chinese habit of eating midnight snacks, shallower boundary layer that inhibited diffusion of pollutants,  
 213 and the lower temperature at night which facilitated semi-volatile compounds from cooking emissions  
 214 to partition into particles resulted in the higher peak concentration at nighttime than at noon (Guo et  
 215 al., 2020).

216 The mass spectrum of HOA (Fig.1b) was characterized with the  $C_nH_{2n-1}^+$  ( $m/z = 27, 41, 55, 69$ )  
 217 and  $C_nH_{2n+1}^+$  ( $m/z = 29, 43, 57, 71$ ) ion species. The concentration of HOA had a good correlation  
 218 with that of primary BC emission ( $R^2=0.74$ ), and also correlated well with that of  $NO_2$  ( $R^2=0.58$ ),

219 indicating considerable impacts of traffic emissions on the HOA mass loading. As shown in Fig.3,  
220 except for summer, HOA increased significantly after sunrise especially in winter, however, began to  
221 decrease in the late evening. HOA was significantly higher during nighttime than during daytime in  
222 all seasons especially in winter, however, was not obvious in summer. HOA mass concentration peaks  
223 around 20:00 LT were attributed to traffic emissions during the nocturnal rush hours. However, the  
224 continuously high concentrations of HOA after 20:00 until 02:00 of the next day might have resulted  
225 from heavy-duty vehicles with daytime traffic restrictions in Guangzhou (Guo et al., 2020;Qin et al.,  
226 2017).

227 Two OOA factors were characterized with high O/C ratio, LOOA with O/C of 0.78 and MOOA  
228 with O/C of 1.2, suggesting high oxidation degrees of SOA factors in Guangzhou urban area, especially  
229 that of MOOA. MOOA and LOOA shared similar diurnal profiles regardless of seasons, with MOOA  
230 showed higher correlations with sulfate and LOOA showed higher correlations with nitrate. MOOA  
231 and LOOA increased together in fall from 09:00 LT until 14:00 LT reached a maximum of 3.7  $\mu\text{g}/\text{m}^3$   
232 for MOOA and 5  $\mu\text{g}/\text{m}^3$  for LOOA, followed by a gradual decrease in SOA concentrations and then  
233 remained relatively flat. The diurnal profiles of SOA in spring and summer were relatively similar to  
234 those in fall, however, more remarkable decreases of SOA from afternoon to midnight were observed  
235 in spring and summer. This is because SOA sometimes increased after sunset in autumn, which was  
236 even more prominent in winter, where LOOA and MOOA would first increase for a while after sunset  
237 and then begun to decrease. However, weaker daytime SOA formation was observed in winter. Note  
238 that a aqSOA factor (called aqOOA in these references) was previously resolved using the aerosol  
239 mass spectrometer measurements (Sun et al., 2016;Zhao et al., 2019) or time-of flight ACSM  
240 measurements (Lei et al., 2021), and the factor was resolved as aqSOA because of its high fraction of  
241 m/z 29 (CHO<sup>+</sup>) and high correlation with sulfate. Both two resolved SOA factors in this study showed  
242 relatively weak correlations with sulfate (Fig.1), and therefore, do not support directly aqueous phase  
243 SOA formation.

## 244 **3 Results and discussion**

### 245 **3.1 The largest contribution of secondary organic aerosols in NR-PM<sub>1</sub>**

246 Time series of the meteorological parameters (including RH, WS and WD), the mass  
247 concentrations of NR-PM<sub>1</sub> and PM<sub>2.5</sub>, chemical compositions of NR-PM<sub>1</sub>, trace gases and four  
248 resolved OA factors are shown Fig.S8. It shows that emission source intensities and meteorological  
249 variables changed dramatically among seasons. Hourly NR-PM<sub>1</sub> mass concentrations ranged from near  
250 zero to 177  $\mu\text{g}/\text{m}^3$  with an average of 21  $\mu\text{g}/\text{m}^3$ . From October to February, northerly winds prevailed  
251 and average NR-PM<sub>1</sub> was relatively higher than that from February to September (26 vs 19  $\mu\text{g}/\text{m}^3$ ),  
252 which were associated with relatively lower boundary height during cold seasons and northern winds  
253 brought polluted continental air mass. While during warm seasons of Guangzhou (March to  
254 September), south-easterly wind prevailed, which brought cleaner air mass from the ocean and the  
255 boundary layer height was higher due to more surface heating. Monthly variations of PM<sub>2.5</sub> are shown  
256 in Fig.4a, PM<sub>2.5</sub> in summer was lowest and around 16  $\mu\text{g}/\text{m}^3$  from May to August which were likely  
257 associated with the prevalence of rainy conditions in summer (Fig.S9) and possibly higher boundary  
258 layer height (Yang et al., 2013). January was the month with highest PM<sub>2.5</sub> mass concentrations with  
259 an average of 49  $\mu\text{g}/\text{m}^3$ , which was consistent with the fact that winter usually experienced the worst  
260 air pollutions due to the stagnant air conditions.

261 The average mass contributions of different components to NR-PM<sub>1</sub> during the entire year and  
262 among different seasons are shown in Fig.4b-4f. On average OA contributed about 50% to NR-PM<sub>1</sub>  
263 with the highest contribution in summer that reached near 57% and lowest contribution in spring of  
264 about 47%. The second largest contributor was sulfate, which on average contributed about 22%, and  
265 more than 20% in spring, summer and fall. However, the contribution of nitrate to NR-PM<sub>1</sub> (23%)  
266 exceeded that of sulfate (14%) and became the second major component after OA in winter, consistent  
267 with the results of Guo et al. (2020) for pollution periods in winter of Guangzhou. The probability  
268 distributions of mass concentrations of OA, sulfate and nitrate are shown in Fig.4g-4i. Both OA and  
269 nitrate were distributed in wide ranges during winter and shared similar shape of probability  
270 distribution, with OA increasing gradually from summer to winter and then reducing in the spring.  
271 Sulfate shared similar magnitudes in summer and winter, and differed much from those in spring and

272 fall that had higher sulfate concentrations and varied in a wider range. Nitrate in summer and fall were  
 273 relatively lower in summer and fall, however, had much higher concentrations in spring and winter.

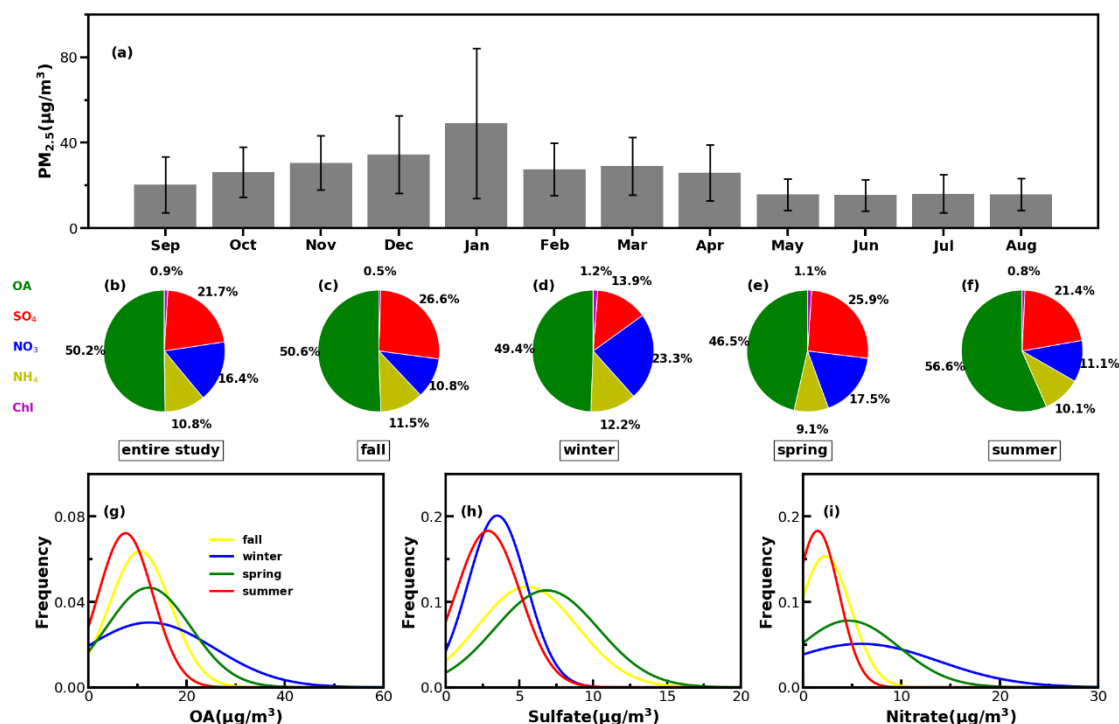


**Figure 4.** (a) Monthly average PM<sub>2.5</sub> mass concentrations from September of 2020 to August of 2021; (b)-(f) The average mass fractions of the chemical components in NR-PM<sub>1</sub> of the entire year and different seasons; (g)-(i) Probability distributions of OA, sulfate (SO<sub>4</sub>) and nitrate (NO<sub>3</sub>) in different seasons.

274 As shown in Fig.5a, average OA concentrations of different months ranged from about 7 µg/m<sup>3</sup>  
 275 to 17 µg/m<sup>3</sup> with the peak in January and the lowest in August, and the variations of OA mass  
 276 concentration in winter and spring were much larger than those in summer and autumn. Monthly  
 277 variations of mass concentrations of the four resolved factors are shown in Fig.5b-5e, and contributions  
 278 of the four OA factors to OA are shown in Fig.5f. In general, HOA remained lower than 2 µg/m<sup>3</sup> in  
 279 most months, however, as the cold season approached from November, the monthly average OA  
 280 increased substantially from about 2 µg/m<sup>3</sup> to near 6 µg/m<sup>3</sup>. The much lower temperature and  
 281 accumulation favorable meteorological conditions likely had resulted in the substantial increase of  
 282 HOA. Compared with HOA, the seasonal variations of COA were less pronounced. The monthly  
 283 average concentration of COA in warm months (February to October) was higher than those in cold  
 284 months (October to January). The lowest monthly average concentration of COA was about 1 µg/m<sup>3</sup>  
 285 which occurred in February when the contribution of COA to OA was near its lowest of about 9%.  
 286 Overall, COA contributed about 19% of OA during the whole year which was close to that of HOA

287 (18%). However, the contributions of COA and HOA to total OA differ much among seasons. The  
 288 contributions of COA to OA were higher than that of HOA during warm months and lower than that  
 289 of HOA in relatively cold months especially in winter. These results highlight the significant  
 290 contributions of POA to OA in Guangzhou urban area, however, contributions of emission sources  
 291 differed much among cold and warm seasons.

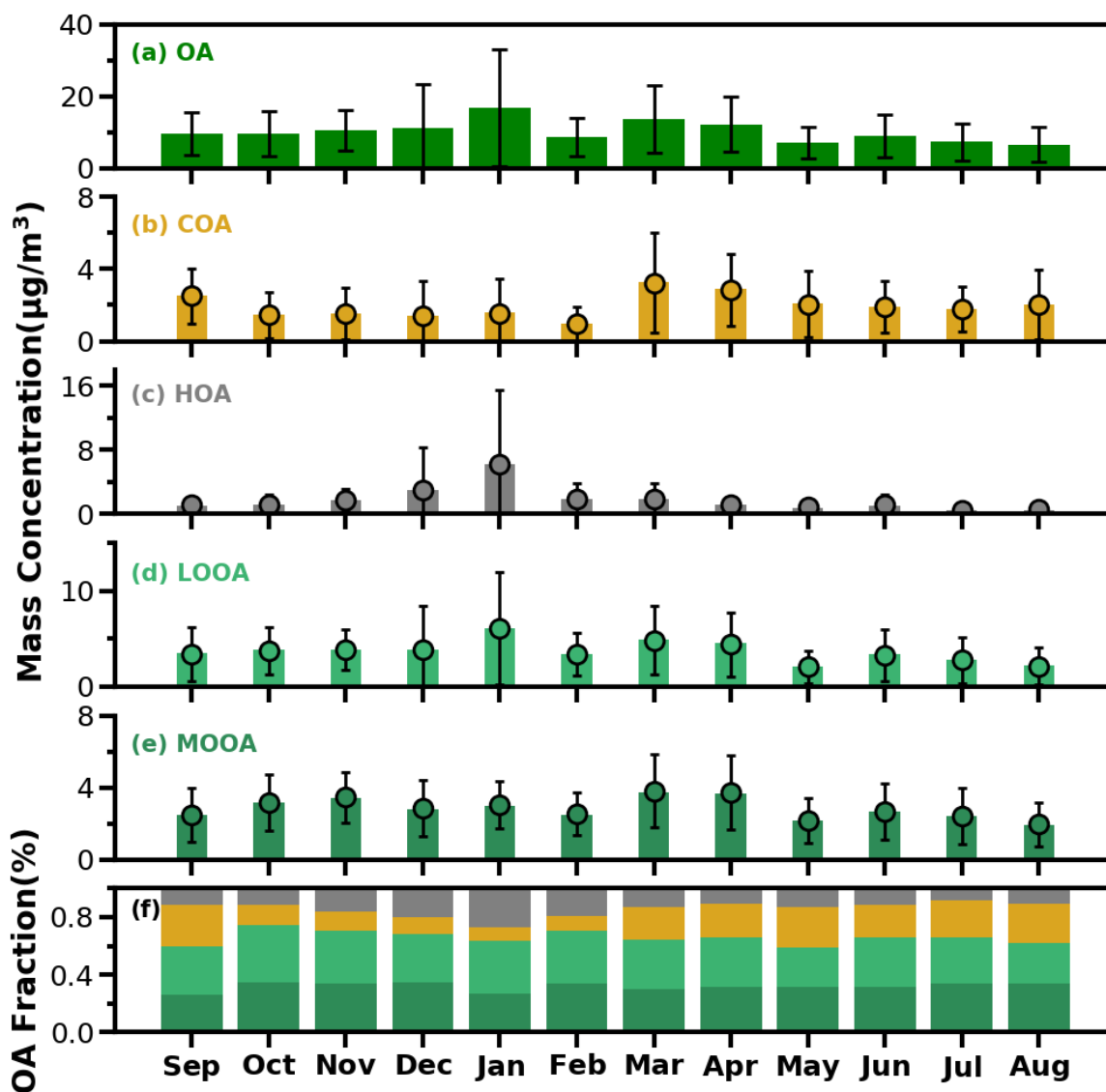


**Figure 5.** The bar plots of monthly average mass concentrations of OA, COA, HOA, LOOA and MOOA from (a) to (e) and mass fractions of OA factors in OA (f).

292 SOA (MOOA+LOOA) contributed more than 60% to OA in all months, reached beyond 70% in  
 293 October and February, and made up on average 63% of OA in the entire year. As shown in Fig.5(e-f),  
 294 LOOA exhibited stronger seasonal variations than MOOA, with monthly average mass concentrations  
 295 of LOOA varying between 2.6 to 6.1  $\mu\text{g}/\text{m}^3$  and monthly average MOOA concentration ranging from

296 2 to 3.8  $\mu\text{g}/\text{m}^3$ . The LOOA mass concentration peaked in the most polluted month of January,  
297 suggesting that significant contributions of LOOA formation to severe haze pollution in winter. The  
298 contribution of LOOA to OA ranged from 27% to 39% with an average of 34%, and the contribution  
299 of MOOA to OA ranged from 26% to 35% with an average of 32%. Overall, the average mass  
300 concentration of SOA was about 1.7 times that of POA for the whole year, and SOA accounted for  
301 about 32% of NR-PM<sub>1</sub>, which was higher than those of sulfate and nitrate, demonstrating the largest  
302 contribution of SOA to NR-PM<sub>1</sub>.

### 303 **3.2 Significant contributions of secondary organic aerosols to haze formations in all seasons**

304 Investigations on contribution variations of aerosol compositions under different aerosol pollution  
305 levels are helpful for understanding mechanisms of haze formations, and results in four seasons are  
306 presented in Fig.6. The chemical composition of NR-PM<sub>1</sub> under different pollution levels differ much  
307 among seasons. In fall, as demonstrated by variations of mass concentrations of aerosol compositions  
308 under different pollution levels shown in Fig.6, pollution conditions in fall were dominantly controlled  
309 by secondary formations of sulfate and SOA, accumulation of primary aerosols and nitrate formation  
310 had relatively smaller impacts. With respect to mass fractions variations, contributions of aerosol  
311 components differed much among different pollution levels. The fraction of OA decreased rapidly from  
312 67% to 50% when the mass concentration of NR-PM<sub>1</sub> gradually increased to 15  $\mu\text{g}/\text{m}^3$ , while the  
313 contribution of sulfate increased substantially from 17% to 30%, and the contribution of nitrate  
314 remained relatively stable at about 10%. When NR-PM<sub>1</sub> further increased, OA contribution remained  
315 relatively flat for NR-PM<sub>1</sub> below about 50  $\mu\text{g}/\text{m}^3$ . Accordingly, the contribution of SO<sub>4</sub><sup>2-</sup> decreased to  
316 ~18%, and the contribution of nitrate substantially increased from ~10 % to 21%. After that, OA  
317 contribution decreased rapidly to about 40% and then remained stable for NR-PM<sub>1</sub> >50  $\mu\text{g}/\text{m}^3$ .  
318 However, the contribution of sulfate began to increase, and the highest contribution could account for  
319 30%, while the contribution of nitrate began to decline gradually to 12%. In addition, the SOA  
320 contributed dominantly to OA (>60%) for NR-PM<sub>1</sub> > 15  $\mu\text{g}/\text{m}^3$  and even reached near 70% for NR-  
321 PM<sub>1</sub> > 35  $\mu\text{g}/\text{m}^3$ , suggesting the dominant role of SOA in OA accumulations in haze events during fall.

322 In winter, haze formations are mostly associated with POA accumulations, SOA and nitrate  
323 formations, with nitrate formation playing the most important role, since it is also accompanied by

324 ammonium formation, while sulfate formation was weak in winter. The fraction of OA increased  
 325 gradually with the increase of NR-PM<sub>1</sub> concentration for NR-PM<sub>1</sub> < 90 μg/m<sup>3</sup> and reached the

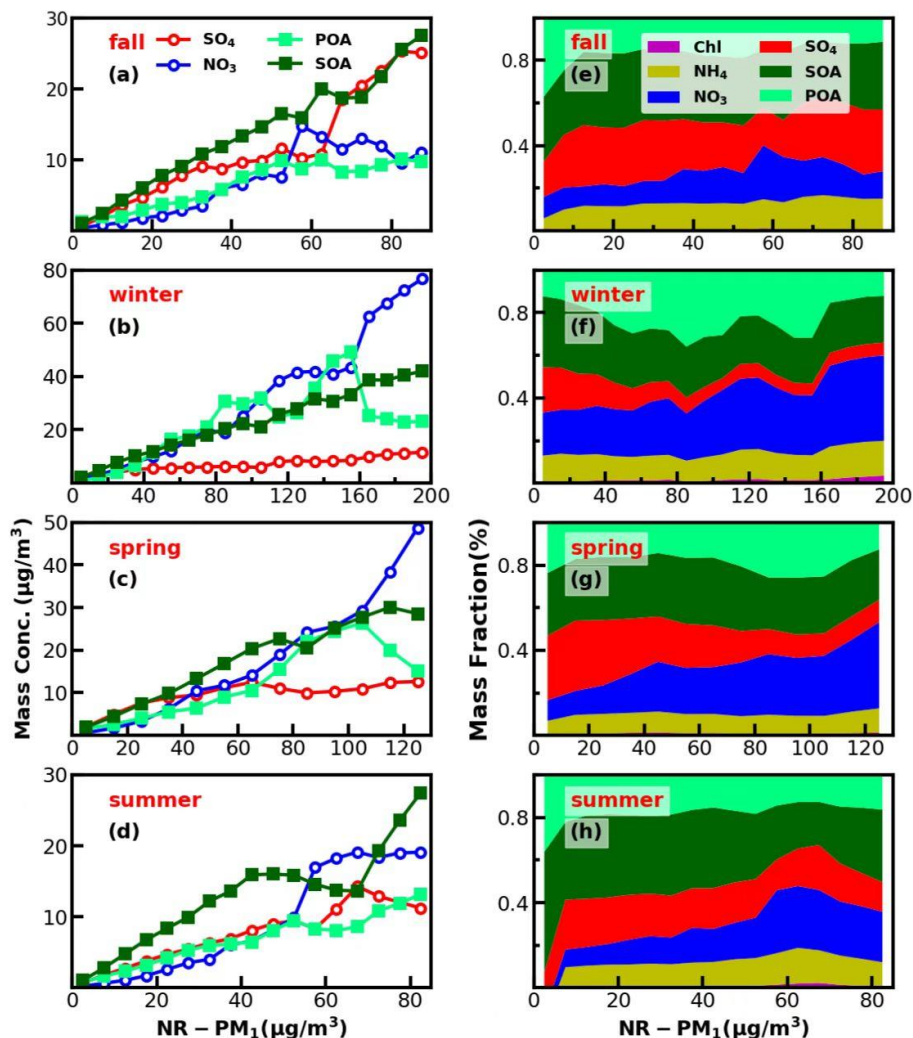


**Figure 6.** Left panels (a-d) show absolute mass concentration variations of aerosol compositions under different NR-PM<sub>1</sub> levels, right panels (e-h) show mass fractions of chemical components as a function of NR-PM<sub>1</sub>.

326 maximum of 60%, while the contribution of nitrate also showed a small increase from 21% to 26%.  
 327 Under aggravating pollution, OA contribution fluctuated, however, showed a decreasing trend from  
 328 60% to ~40%. Meanwhile, the nitrate contribution showed an increasing trend from 26% to ~40%,  
 329 which was similar to that of OA. Sulfate contribution decreased with the increase of NR-PM<sub>1</sub>  
 330 concentration for NR-PM<sub>1</sub> < 100 μg/m<sup>3</sup> and then remained at about 6% as NR-PM<sub>1</sub> increases. In  
 331 addition, the POA contribution increased about 25% to 50% for NR-PM<sub>1</sub> < 100 μg/m<sup>3</sup>. Overall, the  
 332 increase of nitrate, POA and SOA together had resulted in severely polluted conditions in winter. The  
 333 substantial contribution of POA to severe haze demonstrates that meteorological conditions

334 unfavorable for the pollutant diffusion together with the substantial contributions of secondary nitrate  
335 and SOA formations have resulted in the most severe haze pollutions among the year. Especially, HOA  
336 contribution to OA increased from 17% to 52% when NR-PM<sub>1</sub> concentration was less than 140 µg/m<sup>3</sup>,  
337 suggesting the significant role of traffic emission accumulation during severe haze pollution, which  
338 was consistent with results of Yao et al. (2020).

339 In spring, haze pollutions were mostly associated POA accumulation and secondary formations of  
340 nitrate and SOA, especially that of nitrate. The contribution of OA decreased from 51% to 44% as NR-  
341 PM<sub>1</sub> mass concentration increased when NR-PM<sub>1</sub> mass concentration was less than 50 µg/m<sup>3</sup>. When  
342 the mass concentration of NR-PM<sub>1</sub> reached about 105 µg/m<sup>3</sup>, the fraction of OA reached a maximum  
343 of 55%, and then decreased to about 37%. The most noticeable characteristic was the increase of nitrate  
344 contribution (from 10% to 40%) and decrease of sulfate contribution (32% to 10%) as the NR-PM<sub>1</sub>  
345 increased. In summer, secondary aerosol formations contributed dominantly to haze formations, with  
346 POA contribution to NR-PM<sub>1</sub> was about 20% in most conditions. The overall contribution of OA  
347 gradually decreased from near 60% to 35% as the mass concentration of NR-PM<sub>1</sub> increased for NR-  
348 PM<sub>1</sub> concentration < 60 µg/m<sup>3</sup> which was markedly different with those in other seasons, however  
349 increased to 49% as the NR-PM<sub>1</sub> concentration increased further. The contribution of sulfate decreased  
350 from 25% to 13% and the contribution of nitrate increased from 9.0% to 31% with the increase of NR-  
351 PM<sub>1</sub> concentration for NR-PM<sub>1</sub> concentration < 60 µg/m<sup>3</sup>. While the OA was dominated by SOA under  
352 most conditions (about 60%).

353 Overall, haze formation mechanisms differed much among distinct seasons. Sulfate was more  
354 significant than nitrate in fall, while nitrate was more significant than sulfate in spring and winter,  
355 however, SOA contributed significantly to haze formations in all seasons. Note that seasonal variations  
356 of aerosol chemical compositions might differ much among years due to different meteorological  
357 conditions and emissions. For example, the evolution of sulfate during autumn in this study (Fig.S10)  
358 have remarkably different accumulation characteristics from those observed in autumn of 2018 as  
359 shown in Fig.1 of Chen et al. (2021a). However, our conclusions about SOA playing significant roles  
360 in haze formations in Guangzhou urban area during all seasons are consistent among existing literature  
361 (Zhou et al., 2020).

362



363 **3.3 Discussions on SOA formation mechanisms**

364 As shown in Fig.3, both LOOA and MOOA mainly increased after sunrise, highlighting important  
 365 roles of photochemistry in SOA formations. However, as demonstrated by Kuang et al. (2020), the  
 366 daytime SOA formation could be either result from gas-phase photochemistry and subsequent  
 367 condensation (gasSOA), or the result of gas-phase VOCs transformations with subsequent aqueous  
 368 reactions (aqSOA). Especially since the PRD region is characterized by both active photochemistry  
 369 due to strong solar radiation in subtropical regions and high relative humidity (annual average RH of  
 370 ~75%), both photochemistry and aqueous phase reactions might play significant roles in SOA  
 371 formation, however, this aspect was not explored before.

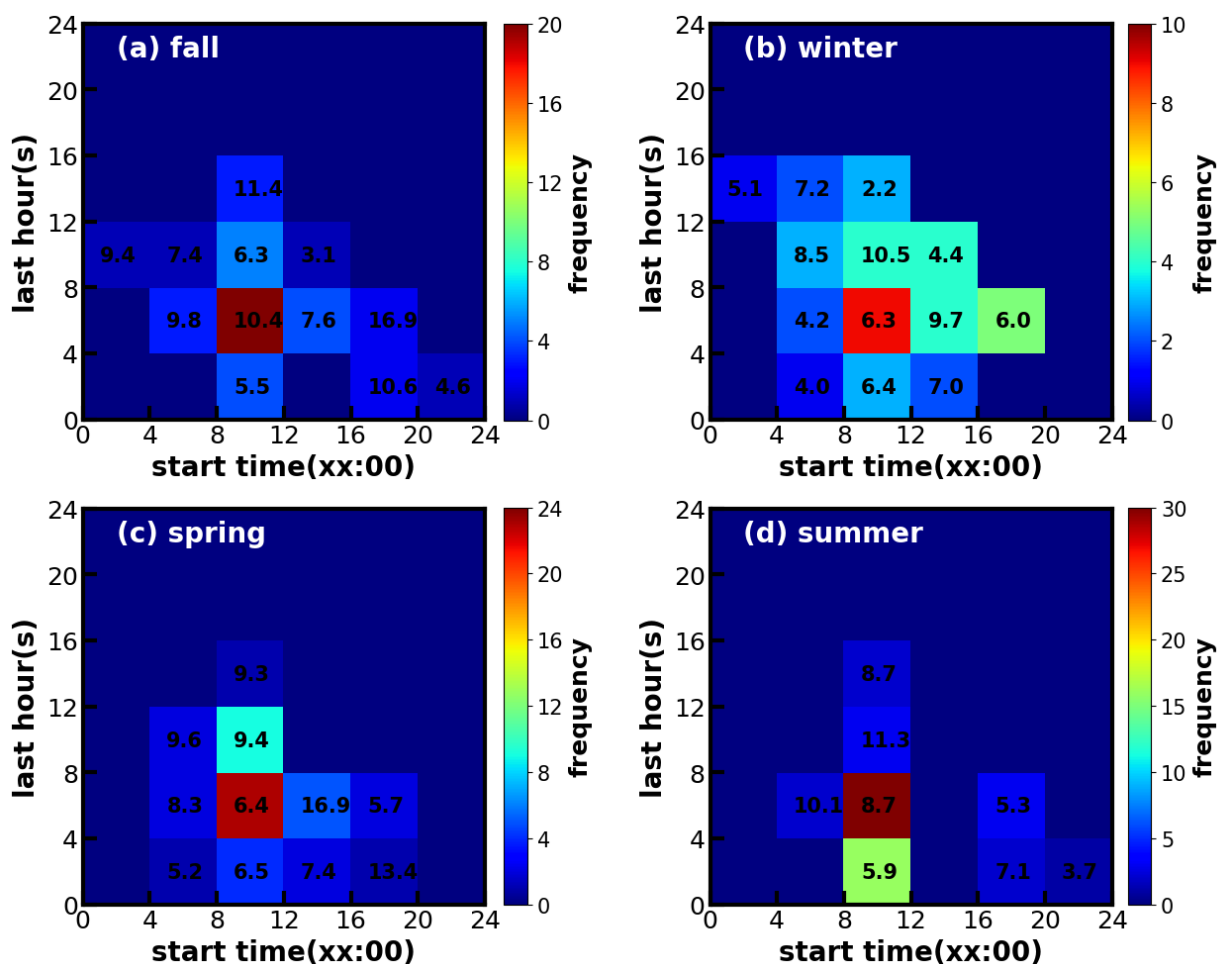


**Figure 7.** Time frequency diagrams of SOA increase events in (a) fall, (b) winter, (c) spring and (d) summer. X-axis represent start time of SOA increase, and y-axis represents the lasting hours of SOA increase events. The color scales indicate the number of occurrences. The values in the grid are the average SOA concentration during the SOA increase case.

372 Considering the frequent co-increase of MOOA and LOOA, they were grouped together as SOA

373 for further investigations on their formation. SOA formation cases in four seasons were identified, the  
374 start time and lasting hours of their occurrences, as well as associated SOA levels are shown in Fig.7.  
375 Note that the identification of SOA formation cases has not considered the dilution effect of the lifting  
376 daytime boundary layer height and was only based on the absolute mass concentration variations.  
377 Therefore, this method has neglected some SOA formation cases that were masked by evolutions of  
378 the boundary layer, and the identified cases represent active SOA formation events that overcame  
379 dilution effects, which might be more suitable for further SOA formation investigations due to strong  
380 SOA formation signals. It shows that in all seasons, the SOA formation happened most frequently  
381 during daytime, starting in the morning and lasting about 4-8 hours. Especially, in spring, summer and  
382 fall, the daytime SOA formation almost happened everyday (Fig.S5-7), even if strong daytime  
383 boundary layer evolutions could be expected in these seasons due to strong surface solar heating, and  
384 resulted in the afternoon SOA mass concentration peaks in these seasons (Fig.3). However, highest  
385 SOA concentrations did not appear in the seasons with the most frequent morning to afternoon  
386 increases. Taking SOA formation cases in spring as an example, if the SOA increase started in the  
387 morning, more than 8 hours duration will result in significant higher SOA concentration. These cases  
388 started in the afternoon and lasted 4-8 hours would result in highest SOA concentration in spring. The  
389 SOA formation cases starting in the morning, however, only lasting within 4 hours, happened  
390 frequently in summer while less in spring and fall, suggesting that the absolute SOA mass  
391 concentration increase was more often stopped by strong boundary layer mixing in summer, which  
392 was consistent with the solar heating characteristics. The highest SOA in fall and winter were  
393 associated with the continuous increase of SOA after sunrise, suggesting that coordination of daytime  
394 and nighttime SOA formation together had resulted in the highest SOA concentrations in fall and winter.

395 To dig deeper into possible mechanisms behind the active daytime SOA formations throughout  
396 the year, we investigated relationships between SOA formation rates and both O<sub>3</sub> as well as aerosol  
397 liquid water content (ALWC) for the most frequent morning to afternoon SOA increase cases. Without  
398 considering the dilution effect of rising boundary layer, the daytime apparent growth rates of SOA  
399 varied from 0.2 to 4.4  $\mu\text{g m}^{-3} \text{h}^{-1}$  (Fig.8). Note that the SOA growth rates was calculated on the basis  
400 of observations of the first four hours for each SOA increase case to reduce impacts of boundary layer  
401 dilution effects. Some previous studies used variations of CO concentrations to partially correct for

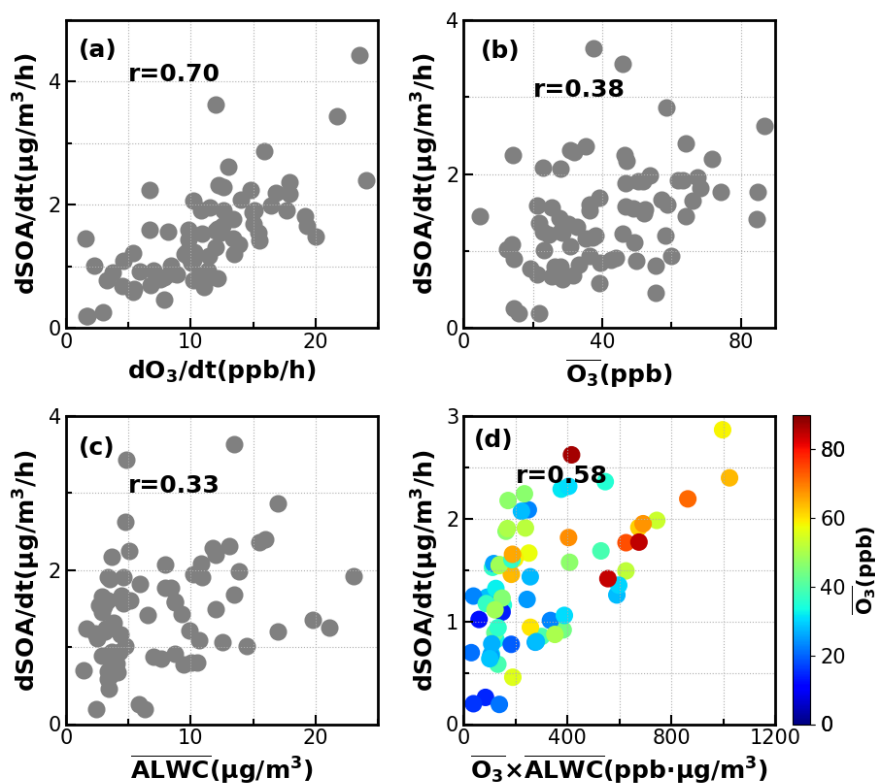


**Figure 8.** Relationships between SOA daytime formation rates with corresponding (a)  $\text{O}_3$  formation rate; (b) average  $\text{O}_3$ ; (c) average ALWC ( $\mu\text{g}/\text{m}^3$ ) and (d) combination of averaged  $\text{O}_3$  and averaged ALWC.

402 boundary layer dilution effects, however this method would fail in sites with strong CO emissions  
 403 (Kuang et al., 2020). The SOA growth rates and were highly correlated to  $\text{O}_3$  formation rates ( $r=0.7$ )  
 404 as shown in Fig.8. However, this result only proved the important role of photochemistry in SOA  
 405 formations. The apparent SOA growth rates showed positive but much weaker correlation with the  
 406 average  $\text{O}_3$  concentration during the period of SOA the increase ( $r=0.38$ ), demonstrating that oxidant  
 407 level was likely not the controlling factor for SOA formation, although  $\text{O}_3$  alone did not represent the  
 408 variations of oxidation levels and other sources such as HONO photolysis (Yu et al., 2022) also  
 409 contribute to OH radicals and is a typical oxidant in daytime photochemistry. To investigate the  
 410 possible roles of aqueous reactions in SOA formation, the relationship between apparent SOA rates  
 411 and corresponding average ALWC were also investigated, and a positive but weak correlation was  
 412 found ( $r=0.33$ ). More importantly, the correlation coefficient between apparent SOA growth rates and  
 413 the variable of average ALWC multiplying by average  $\text{O}_3$  would be much higher ( $r=0.58$ , Fig.8d),  
 414 suggesting that the coordination of gas-phase photochemistry and further aqueous reactions had likely  
 415 resulted in the rapid daytime SOA formations.

416 Besides the daytime SOA formation associated with photochemistry, dark transformations of  
 417 VOCs that involve nighttime gas-phase and aqueous phase reactions might also result in efficient SOA  
 418 formations. As shown in Fig.7, continuous increases of SOA were also frequently observed after sunset

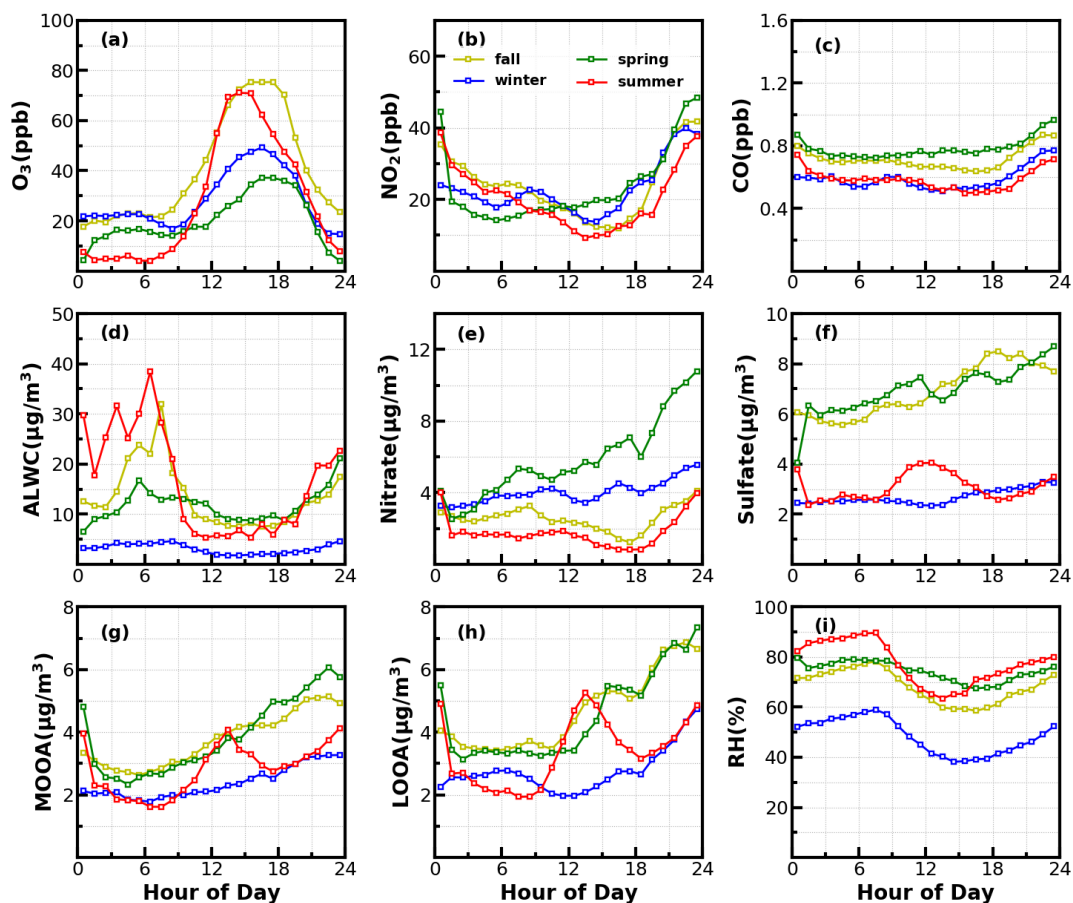


**Figure 9.** Average diurnal variations of (a) O<sub>3</sub>; (b) NO<sub>2</sub>; (c) CO; (d) ALWC; (e) nitrate; (f) sulfate; (g) MOOA; (h) LOOA and (i) RH for identified days with nighttime SOA increases.

419 in spring (17 days), fall (18 days) and winter (20 days) with sporadic occurrence in summer, and the  
 420 coordination of daytime and nighttime SOA formations together have resulted in the highest SOA  
 421 concentrations in fall and winter which were associated with severe haze pollutions as demonstrated  
 422 above. Average diurnal profiles of O<sub>3</sub>, NO<sub>2</sub>, CO, RH, ALWC, nitrate, sulfate, LOOA and MOOA for  
 423 cases with co-increases of LOOA and MOOA after 18:00 in different seasons are shown in Fig.9. On  
 424 average, SOA usually showed decreases during nighttime (Fig.3) due to transport of air mass from  
 425 cleaner suburban regions. The average wind speed was 1.7 m/s from 18:00 to 23:00 LT for identified  
 426 nighttime SOA increase cases and was obviously lower than the corresponding average wind speed of  
 427 2.3 m/s, suggesting the more stagnant air mass tended to favor the nighttime SOA increases. However,

428 the nighttime 5h back trajectories shown in Fig.S11 demonstrated that the nighttime replacement of  
 429 surrounding suburban cleaner air mass still prevailed, therefore the continuous increases of SOA  
 430 suggested that nighttime SOA formation occurred on a regional scale. The increases of LOOA and  
 431 MOOA were accompanied with obvious nitrate formation in all seasons as well as slight increases of  
 432 sulfate, further indicating for regional scale nighttime secondary aerosol formations during these  
 433 nighttime SOA formation events. Except for summer, continuous increase of SOA from the morning  
 434 to nighttime confirmed that the coordination of daytime and nighttime SOA formations had contributed  
 435 to haze formations. Number of days for daily average NR-PM<sub>1</sub> ranges of 0-20, 20-35, 35-45, 45-60  
 436 and >60  $\mu\text{g}/\text{m}^3$  were 185,85,24,10 and 7, respectively (Fig.10a). All cases with daily average NR-PM<sub>1</sub>  
 437 higher than 45  $\mu\text{g}/\text{m}^3$  occurred in fall, winter and spring. The corresponding average diurnal variations  
 438 of SOA for these relatively severe conditions shown in Fig.10b confirmed further that the coordination

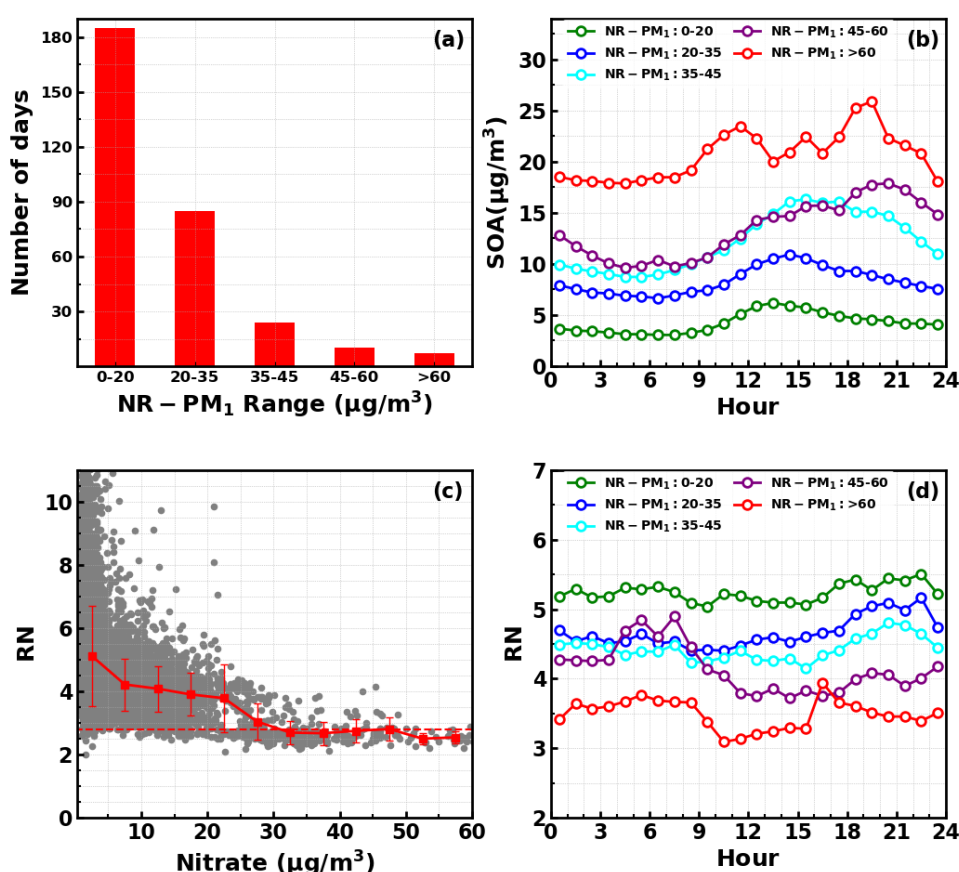


**Figure 10.** (a) Number of days in different daily average NR-PM<sub>1</sub> ranges; (b) Diurnal profiles of SOA under different NR-PM<sub>1</sub> ranges; (c) Variations NO<sup>+</sup>/NO<sub>2</sub><sup>+</sup> (RN) as a function of measured nitrate, horizontal dashed line corresponds to RN of 2.8, red markers and bars represents averages and standard deviations; (d) Diurnal profiles of RN under different NR-PM<sub>1</sub> ranges.

439 of daytime and nighttime SOA formations had contributed to severe haze formations in Guangzhou  
440 urban area.

441 The  $\text{NO}_3$  radical formed through the reaction between  $\text{NO}_2$  and  $\text{O}_3$  is the typical nighttime oxidant.  
442 Results of Rollins et al. (2012) and Kiendler-Scharr et al. (2016) revealed that  $\text{NO}_3$  oxidation of VOCs  
443 would contribute substantially to nighttime SOA increase. As shown in Fig.9a, after sunset, the  $\text{O}_3$   
444 concentration decreased quickly, however, remained substantially higher than zero, accompanied was  
445 the remarkable increases of  $\text{NO}_2$  and nitrate. In Guangzhou urban areas, nitrate can either be formed  
446 through gas-phase oxidation of  $\text{NO}_2$  by OH which forms  $\text{HNO}_3$  and then condenses onto aerosol phase,  
447 or be formed through the hydrolysis of  $\text{N}_2\text{O}_5$ , which is formed through reactions between  $\text{NO}_2$  and  
448  $\text{NO}_3$  radical (Yang et al., 2022). The obvious co-increases in nitrate and SOA after sunset indicated  
449 that the decrease of  $\text{O}_3$  and increase of  $\text{NO}_2$  consumption had supplied the  $\text{NO}_3$  and  $\text{N}_2\text{O}_5$  reaction  
450 chains and the increase of ALWC favored the hydrolysis of  $\text{N}_2\text{O}_5$ . This was indirectly confirmed when  
451 during winter, despite relatively high concentrations of  $\text{O}_3$  and  $\text{NO}_2$  after sunrise compared with other  
452 seasons, nitrate formation was much less prominent due to substantially lower ALWC associated with  
453 lower RH. However, the quick increase of SOA still occurred after sunset despite weak daytime SOA  
454 formation, suggesting that aqueous reactions might play minor roles in nighttime SOA formation that  
455 involve  $\text{NO}_3$  radical in Guangzhou urban area. The nighttime chemistry that involves  $\text{NO}_3$  radical  
456 might contribute substantially to organic nitrate formation (Ng et al., 2008; Fry et al., 2009; Rollins et  
457 al., 2012) which would produce the same ions ( $\text{NO}^+$  and  $\text{NO}_2^+$ ) with inorganic nitrate due to the  
458 fragmentation of nitrate functionality (-ONO<sub>2</sub>) under 70 eV electron ionization in the aerosol mass  
459 spectrometer measurements. However, organic nitrate has different fragmentation pattern with that of  
460 inorganic nitrate with previous laboratory studies have shown that the  $\text{RN}=\text{NO}^+/\text{NO}_2^+$  of organic  
461 nitrate is substantially higher than that of inorganic nitrate. Farmer et al. (2010) thus proposed that the  
462 RN variations can be used as an indicator of organic nitrate formations. The Q-ACSM measurements  
463 with unit mass resolution cannot provide accurate measurements of RN due to the resolution limitation  
464 (Allan et al., 2004), however, the resolved RN related to measured nitrate might provide qualitative  
465 constraints on impacts of organic nitrates. The variations of resolved RN as a function of measured  
466 nitrate are shown in Fig.10c, which shows that at high levels of nitrate when inorganic nitrate usually  
467 dominates (Xu et al., 2021), the RN approaches near 2.8 which was close to the inorganic nitrate RN

468 reported in (Xu et al., 2021), and locates in the range of 1.1-3.5 of inorganic nitrate RN reported in  
469 literatures (Xu et al., 2015). Diurnal variations of RN under different pollution levels shown in Fig.10d  
470 reveals higher nighttime RN than daytime, and obvious continuous increase of RN after sunset can be  
471 observed for relatively clean and polluted conditions (daily average NR-PM<sub>1</sub> of 20-35 μg/m<sup>3</sup> to NR-  
472 PM<sub>1</sub> of 45-60 μg/m<sup>3</sup>), suggesting active nighttime organic nitrate formations, which confirmed the  
473 involvement of NO<sub>3</sub> radicals in nighttime SOA formations.

#### 474 **4 Implications for future studies**

475 In this study, we highlighted the significant roles of SOA in haze formations in Guangzhou urban  
476 area during the entire year and pointed out that for the most prominent and frequent daytime SOA  
477 formations all the year around, both gas-phase photochemistry and aqueous reactions played  
478 significant roles. Therefore, daytime SOA formation was weak in winter when oxidant level and RH  
479 were low, whereas prominent SOA formations were be observed in fall, spring and summer on almost  
480 daily basis. However, how gas-phase and aqueous phase reactions have coordinated to promote the  
481 SOA formation, and the different contributions of gasSOA and aqSOA to SOA formations under  
482 different meteorological conditions and VOCs profiles in different seasons are not clear. In addition,  
483 our results suggested that the coordination of daytime and nighttime SOA formation together had  
484 resulted in highest SOA concentrations in Guangzhou urban area, thus contributed significantly to  
485 severe haze formation. The co-increases of nitrate and SOA after sunrise indicated the significant roles  
486 of nighttime NO<sub>3</sub> radical chemistry in promoting haze formations. However, our understanding on  
487 how nighttime chemistry evolved and contributed to secondary aerosols formations in different  
488 seasons is still highly insufficient in this region. Therefore, the precursors and formation pathways of  
489 daytime and nighttime SOA formations and how they coordinated to promote severe haze formations  
490 need further comprehensive investigations to make targeted emission control strategies to continuously  
491 improve air quality in the PRD region. Also, findings of this study have important implications on  
492 future investigations of SOA formation mechanisms in urban areas of southern China that share similar  
493 emission sources and meteorological conditions.

494

495 **Data availability.** All data needed are presented in time series of Figures and supplementary Figures,

496 raw datasets of this study are available from the corresponding author Li Liu (liul@gd121.cn) upon  
497 request.

498

499 **Competing interests.** The authors declare that they have no conflict of interest.

500

501 **Author Contributions.** YK and LL designed the aerosol experiments. YK conceived and led this  
502 research. MMZ and YK wrote the manuscript. MMZ and LL conducted the long-term Q-ACSM  
503 measurements. MMZ and YH performed the PMF analysis. HBX, CY, YZ and FL helped maintain and  
504 calibrating the Q-ACSM. CL provided meteorological datasets, BL performed the AE33 measurements  
505 and post data processing. XJD obtained funding for the continuous aerosol measurements. JCT and  
506 WYX provided insights into data analysis, and all authors contributed to revisions of this paper.

507

508

## 509 **Acknowledgments**

510 This work is supported by the Guangdong Provincial Key Research and Development Program  
511 (2020B1111360003); National Natural Science Foundation of China (42175083 and 42105092);  
512 Guangdong Basic and Applied Basic Research Foundation (2019A1515110791 and  
513 2019A1515011808); National Key Research and Development Program of China (2019YFCO214605);  
514 Science and Technology Innovation Team Plan of Guangdong Meteorological Bureau  
515 (GRMCTD202003). The Special Fund Project for Science and Technology Innovation Strategy of  
516 Guangdong Province (Grant No.2019B121205004).

517

## 518 **References**

519 Allan, J. D., Delia, A. E., Coe, H., Bower, K. N., Alfarra, M. R., Jimenez, J. L., Middlebrook, A. M., Drewnick, F., Onasch,  
520 T. B., Canagaratna, M. R., Jayne, J. T., and Worsnop, D. R.: A generalised method for the extraction of chemically  
521 resolved mass spectra from Aerodyne aerosol mass spectrometer data, *Journal of Aerosol Science*, 35, 909-922,  
522 <https://doi.org/10.1016/j.jaerosci.2004.02.007>, 2004.  
523 Canagaratna, M. R., Jayne, J. T., Jimenez, J. L., Allan, J. D., Alfarra, M. R., Zhang, Q., Onasch, T. B., Drewnick, F., Coe,



524 H., Middlebrook, A., Delia, A., Williams, L. R., Trimborn, A. M., Northway, M. J., DeCarlo, P. F., Kolb, C. E., Davidovits,  
525 P., and Worsnop, D. R.: Chemical and microphysical characterization of ambient aerosols with the aerodyne aerosol  
526 mass spectrometer, *Mass Spectrom Rev*, 26, 185-222, 10.1002/mas.20115, 2007.

527 Canonaco, F., Crippa, M., Slowik, J. G., Baltensperger, U., and Prevot, A. S. H.: SoFi, an IGOR-based interface for the  
528 efficient use of the generalized multilinear engine (ME-2) for the source apportionment: ME-2 application to  
529 aerosol mass spectrometer data, *Atmos. Meas. Tech.*, 6, 3649-3661, 10.5194/amt-6-3649-2013, 2013.

530 Canonaco, F., Tobler, A., Chen, G., Sosedova, Y., Slowik, J. G., Bozzetti, C., Daellenbach, K. R., El Haddad, I., Crippa,  
531 M., Huang, R. J., Furger, M., Baltensperger, U., and Prévôt, A. S. H.: A new method for long-term source  
532 apportionment with time-dependent factor profiles and uncertainty assessment using SoFi Pro: application to 1  
533 year of organic aerosol data, *Atmos. Meas. Tech.*, 14, 923-943, 10.5194/amt-14-923-2021, 2021.

534 Chen, W., Ye, Y., Hu, W., Zhou, H., Pan, T., Wang, Y., Song, W., Song, Q., Ye, C., Wang, C., Wang, B., Huang, S., Yuan,  
535 B., Zhu, M., Lian, X., Zhang, G., Bi, X., Jiang, F., Liu, J., Canonaco, F., Prevot, A. S. H., Shao, M., and Wang, X.: Real-  
536 Time Characterization of Aerosol Compositions, Sources, and Aging Processes in Guangzhou During PRIDE-GBA  
537 2018 Campaign, *Journal of Geophysical Research: Atmospheres*, 126, e2021JD035114,  
538 <https://doi.org/10.1029/2021JD035114>, 2021a.

539 Chen, W., Ye, Y. Q., Hu, W. W., Zhou, H. S., Pan, T. L., Wang, Y. K., Song, W., Song, Q. C., Ye, C. S., Wang, C. M.,  
540 Wang, B. L., Huang, S., Yuan, B., Zhu, M., Lian, X. F., Zhang, G. H., Bi, X. H., Jiang, F., Liu, J. W., Canonaco, F., Prevot,  
541 A. S. H., Shao, M., and Wang, X. M.: Real-Time Characterization of Aerosol Compositions, Sources, and Aging  
542 Processes in Guangzhou During PRIDE-GBA 2018 Campaign, *J Geophys Res-Atmos*, 126, ARTN e2021JDO35114  
543 10.1029/2021JD035114, 2021b.

544 Drinovec, L., Močnik, G., Zotter, P., Prévôt, A. S. H., Ruckstuhl, C., Coz, E., Rupakheti, M., Sciare, J., Müller, T.,  
545 Wiedensohler, A., and Hansen, A. D. A.: The "dual-spot" Aethalometer: an improved measurement of aerosol black  
546 carbon with real-time loading compensation, *Atmospheric Measurement Techniques*, 8, 1965-1979, 10.5194/amt-  
547 8-1965-2015, 2015.

548 Ervens, B., Turpin, B. J., and Weber, R. J.: Secondary organic aerosol formation in cloud droplets and aqueous  
549 particles (aqSOA): a review of laboratory, field and model studies, *Atmos. Chem. Phys.*, 11, 11069-11102,  
550 10.5194/acp-11-11069-2011, 2011.

551 Farmer, D. K., Matsunaga, A., Docherty, K. S., Surratt, J. D., Seinfeld, J. H., Ziemann, P. J., and Jimenez, J. L.: Response  
552 of an aerosol mass spectrometer to organonitrates and organosulfates and implications for atmospheric chemistry,  
553 *Proceedings of the National Academy of Sciences*, 107, 6670-6675, doi:10.1073/pnas.0912340107, 2010.

554 Fry, J. L., Kiendler-Scharr, A., Rollins, A. W., Wooldridge, P. J., Brown, S. S., Fuchs, H., Dubé, W., Mensah, A., dal Maso,  
555 M., Tillmann, R., Dorn, H. P., Brauers, T., and Cohen, R. C.: Organic nitrate and secondary organic aerosol yield from  
556 NO<sub>3</sub> oxidation of β-pinene evaluated using a gas-phase kinetics/aerosol partitioning model, *Atmos.*  
557 *Chem. Phys.*, 9, 1431-1449, 10.5194/acp-9-1431-2009, 2009.

558 Guo, H., Liu, J., Froyd, K. D., Roberts, J. M., Veres, P. R., Hayes, P. L., Jimenez, J. L., Nenes, A., and Weber, R. J.: Fine  
559 particle pH and gas-particle phase partitioning of inorganic species in Pasadena, California, during the 2010 CalNex  
560 campaign, *Atmospheric Chemistry and Physics*, 17, 5703-5719, 10.5194/acp-17-5703-2017, 2017.

561 Guo, J. C., Zhou, S. Z., Cai, M. F., Zhao, J., Song, W., Zhao, W. X., Hu, W. W., Sun, Y. L., He, Y., Yang, C. Q., Xu, X. Z.,  
562 Zhang, Z. S., Cheng, P., Fan, Q., Hang, J., Fan, S. J., Wang, X. M., and Wang, X. M.: Characterization of submicron  
563 particles by time-of-flight aerosol chemical speciation monitor (ToF-ACSM) during wintertime: aerosol  
564 composition, sources, and chemical processes in Guangzhou, China, *Atmospheric Chemistry and Physics*, 20, 7595-  
565 7615, 10.5194/acp-20-7595-2020, 2020.

566 He, L. Y., Huang, X. F., Xue, L., Hu, M., Lin, Y., Zheng, J., Zhang, R. Y., and Zhang, Y. H.: Submicron aerosol analysis  
567 and organic source apportionment in an urban atmosphere in Pearl River Delta of China using high-resolution

568 aerosol mass spectrometry, *J Geophys Res-Atmos*, 116, Artn D12304  
569 10.1029/2010jd014566, 2011.

570 Huang, X., Ding, A., Gao, J., Zheng, B., Zhou, D., Qi, X., Tang, R., Wang, J., Ren, C., Nie, W., Chi, X., Xu, Z., Chen, L.,  
571 Li, Y., Che, F., Pang, N., Wang, H., Tong, D., Qin, W., Cheng, W., Liu, W., Fu, Q., Liu, B., Chai, F., Davis, S. J., Zhang, Q.,  
572 and He, K.: Enhanced secondary pollution offset reduction of primary emissions during COVID-19 lockdown in  
573 China, *National Science Review*, 8, nwa137, 10.1093/nsr/nwa137, 2021.

574 Huang, X. F., He, L. Y., Hu, M., Canagaratna, M. R., Kroll, J. H., Ng, N. L., Zhang, Y. H., Lin, Y., Xue, L., Sun, T. L., Liu, X.  
575 G., Shao, M., Jayne, J. T., and Worsnop, D. R.: Characterization of submicron aerosols at a rural site in Pearl River  
576 Delta of China using an Aerodyne High-Resolution Aerosol Mass Spectrometer, *Atmospheric Chemistry and Physics*,  
577 11, 1865-1877, 10.5194/acp-11-1865-2011, 2011.

578 Jayne, J. T., Leard, D. C., Zhang, X. F., Davidovits, P., Smith, K. A., Kolb, C. E., and Worsnop, D. R.: Development of an  
579 aerosol mass spectrometer for size and composition analysis of submicron particles, *Aerosol Science and  
580 Technology*, 33, 49-70, Doi 10.1080/027868200410840, 2000.

581 Jimenez, J. L., Jayne, J. T., Shi, Q., Kolb, C. E., Worsnop, D. R., Yourshaw, I., Seinfeld, J. H., Flagan, R. C., Zhang, X. F.,  
582 Smith, K. A., Morris, J. W., and Davidovits, P.: Ambient aerosol sampling using the Aerodyne Aerosol Mass  
583 Spectrometer, *J Geophys Res-Atmos*, 108, Artn 8425  
584 10.1029/2001jd001213, 2003.

585 Jimenez, J. L., Canagaratna, M. R., Donahue, N. M., Prevot, A. S. H., Zhang, Q., Kroll, J. H., DeCarlo, P. F., Allan, J. D.,  
586 Coe, H., Ng, N. L., Aiken, A. C., Docherty, K. S., Ulbrich, I. M., Grieshop, A. P., Robinson, A. L., Duplissy, J., Smith, J. D.,  
587 Wilson, K. R., Lanz, V. A., Hueglin, C., Sun, Y. L., Tian, J., Laaksonen, A., Raatikainen, T., Rautiainen, J., Vaattovaara, P.,  
588 Ehn, M., Kulmala, M., Tomlinson, J. M., Collins, D. R., Cubison, M. J., Dunlea, J., Huffman, J. A., Onasch, T. B., Alfarra,  
589 M. R., Williams, P. I., Bower, K., Kondo, Y., Schneider, J., Drewnick, F., Borrmann, S., Weimer, S., Demerjian, K., Salcedo,  
590 D., Cottrell, L., Griffin, R., Takami, A., Miyoshi, T., Hatakeyama, S., Shimono, A., Sun, J. Y., Zhang, Y. M., Dzepina, K.,  
591 Kimmel, J. R., Sueper, D., Jayne, J. T., Herndon, S. C., Trimborn, A. M., Williams, L. R., Wood, E. C., Middlebrook, A.  
592 M., Kolb, C. E., Baltensperger, U., and Worsnop, D. R.: Evolution of Organic Aerosols in the Atmosphere, *Science*,  
593 326, 1525-1529, 10.1126/science.1180353, 2009.

594 Kiendler-Scharr, A., Mensah, A. A., Friese, E., Topping, D., Nemitz, E., Prevot, A. S. H., Äijälä, M., Allan, J., Canonaco,  
595 F., Canagaratna, M., Carbone, S., Crippa, M., Dall'Osto, M., Day, D. A., De Carlo, P., Di Marco, C. F., Elbern, H., Eriksson,  
596 A., Freney, E., Hao, L., Herrmann, H., Hildebrandt, L., Hillamo, R., Jimenez, J. L., Laaksonen, A., McFiggans, G., Mohr,  
597 C., O'Dowd, C., Otjes, R., Ovadnevaite, J., Pandis, S. N., Poulain, L., Schlag, P., Sellegri, K., Swietlicki, E., Tiitta, P.,  
598 Vermeulen, A., Wahner, A., Worsnop, D., and Wu, H.-C.: Ubiquity of organic nitrates from nighttime chemistry in  
599 the European submicron aerosol, *Geophysical Research Letters*, 43, 7735-7744, 10.1002/2016gl069239, 2016.

600 Kuang, Y., He, Y., Xu, W., Yuan, B., Zhang, G., Ma, Z., Wu, C., Wang, C., Wang, S., Zhang, S., Tao, J., Ma, N., Su, H.,  
601 Cheng, Y., Shao, M., and Sun, Y.: Photochemical Aqueous-Phase Reactions Induce Rapid Daytime Formation of  
602 Oxygenated Organic Aerosol on the North China Plain, *Environmental science & technology*, 54, 3849-3860,  
603 10.1021/acs.est.9b06836, 2020.

604 Lei, L., Sun, Y., Ouyang, B., Qiu, Y., Xie, C., Tang, G., Zhou, W., He, Y., Wang, Q., Cheng, X., Fu, P., and Wang, Z.:  
605 Vertical Distributions of Primary and Secondary Aerosols in Urban Boundary Layer: Insights into Sources, Chemistry,  
606 and Interaction with Meteorology, *Environmental science & technology*, 55, 4542-4552, 10.1021/acs.est.1c00479,  
607 2021.

608 Li, Y. J., Lee, B. P., Su, L., Fung, J. C. H., and Chan, C. K.: Seasonal characteristics of fine particulate matter (PM) based  
609 on high-resolution time-of-flight aerosol mass spectrometric (HR-ToF-AMS) measurements at the HKUST  
610 Supersite in Hong Kong, *Atmos. Chem. Phys.*, 15, 37-53, 10.5194/acp-15-37-2015, 2015.

611 Li, Z., Lei, L., Li, Y., Chen, C., Wang, Q., Zhou, W., Sun, J., Xie, C., and Sun, Y.: Aerosol characterization in a city in

612 central China plain and implications for emission control, *J Environ Sci (China)*, 104, 242-252,  
613 10.1016/j.jes.2020.11.015, 2021.

614 Liu, L., Kuang, Y., Zhai, M., Xue, B., He, Y., Tao, J., Luo, B., Xu, W., Tao, J., Yin, C., Li, F., Xu, H., Deng, T., Deng, X., Tan,  
615 H., and Shao, M.: Strong light scattering of highly oxygenated organic aerosols impacts significantly on visibility  
616 degradation, *Atmos. Chem. Phys.*, 22, 7713-7726, 10.5194/acp-22-7713-2022, 2022.

617 Middlebrook, A. M., Bahreini, R., Jimenez, J. L., and Canagaratna, M. R.: Evaluation of Composition-Dependent  
618 Collection Efficiencies for the Aerodyne Aerosol Mass Spectrometer using Field Data, *Aerosol Science and  
619 Technology*, 46, 258-271, 10.1080/02786826.2011.620041, 2012.

620 Mohr, C., DeCarlo, P. F., Heringa, M. F., Chirico, R., Slowik, J. G., Richter, R., Reche, C., Alastuey, A., Querol, X., Seco,  
621 R., Penuelas, J., Jimenez, J. L., Crippa, M., Zimmermann, R., Baltensperger, U., and Prevot, A. S. H.: Identification and  
622 quantification of organic aerosol from cooking and other sources in Barcelona using aerosol mass spectrometer  
623 data, *Atmospheric Chemistry and Physics*, 12, 1649-1665, 10.5194/acp-12-1649-2012, 2012.

624 Ng, N. L., Kwan, A. J., Surratt, J. D., Chan, A. W. H., Chhabra, P. S., Sorooshian, A., Pye, H. O. T., Crouse, J. D.,  
625 Wennberg, P. O., Flagan, R. C., and Seinfeld, J. H.: Secondary organic aerosol (SOA) formation from reaction of  
626 isoprene with nitrate radicals (NO<sub>3</sub>), *Atmos. Chem. Phys.*, 8, 4117-4140, 10.5194/acp-8-4117-2008,  
627 2008.

628 Ng, N. L., Herndon, S. C., Trimborn, A., Canagaratna, M. R., Croteau, P. L., Onasch, T. B., Sueper, D., Worsnop, D. R.,  
629 Zhang, Q., Sun, Y. L., and Jayne, J. T.: An Aerosol Chemical Speciation Monitor (ACSM) for Routine Monitoring of  
630 the Composition and Mass Concentrations of Ambient Aerosol, *Aerosol Science and Technology*, 45, 780-794, Pii  
631 934555189  
632 10.1080/02786826.2011.560211, 2011.

633 Paatero, P.: The Multilinear Engine—A Table-Driven, Least Squares Program for Solving Multilinear Problems,  
634 Including then-Way Parallel Factor Analysis Model, *Journal of Computational and Graphical Statistics*, 8, 854-888,  
635 10.1080/10618600.1999.10474853, 1999.

636 Qin, Y. M., Tan, H. B., Li, Y. J., Schurman, M. I., Li, F., Canonaco, F., Prevot, A. S. H., and Chan, C. K.: Impacts of traffic  
637 emissions on atmospheric particulate nitrate and organics at a downwind site on the periphery of Guangzhou,  
638 China, *Atmospheric Chemistry and Physics*, 17, 10245-10258, 10.5194/acp-17-10245-2017, 2017.

639 Rollins, A. W., Browne, E. C., Min, K. E., Pusede, S. E., Wooldridge, P. J., Gentner, D. R., Goldstein, A. H., Liu, S., Day,  
640 D. A., Russell, L. M., and Cohen, R. C.: Evidence for NO<sub>x</sub> Control over  
641 Nighttime SOA Formation, *Science*, 337, 1210, 10.1126/science.1221520, 2012.

642 Su, H., Cheng, Y., and Pöschl, U.: New Multiphase Chemical Processes Influencing Atmospheric Aerosols, Air Quality,  
643 and Climate in the Anthropocene, *Accounts of chemical research*, 53, 2034-2043, 10.1021/acs.accounts.0c00246,  
644 2020.

645 Sun, Y., Du, W., Fu, P., Wang, Q., Li, J., Ge, X., Zhang, Q., Zhu, C., Ren, L., Xu, W., Zhao, J., Han, T., Worsnop, D. R.,  
646 and Wang, Z.: Primary and secondary aerosols in Beijing in winter: sources, variations and processes, *Atmos. Chem.  
647 Phys.*, 16, 8309-8329, 10.5194/acp-16-8309-2016, 2016.

648 Sun, Y. L., Zhang, Q., Schwab, J. J., Demerjian, K. L., Chen, W. N., Bae, M. S., Hung, H. M., Hogrefe, O., Frank, B.,  
649 Rattigan, O. V., and Lin, Y. C.: Characterization of the sources and processes of organic and inorganic aerosols in  
650 New York city with a high-resolution time-of-flight aerosol mass spectrometer, *Atmospheric Chemistry and Physics*,  
651 11, 1581-1602, 10.5194/acp-11-1581-2011, 2011.

652 Sun, Y. L., Wang, Z. F., Dong, H. B., Yang, T., Li, J., Pan, X. L., Chen, P., and Jayne, J. T.: Characterization of summer  
653 organic and inorganic aerosols in Beijing, China with an Aerosol Chemical Speciation Monitor, *Atmos. Environ.*, 51,  
654 250-259, 10.1016/j.atmosenv.2012.01.013, 2012.

655 Sun, Y. L., Wang, Z. F., Fu, P. Q., Yang, T., Jiang, Q., Dong, H. B., Li, J., and Jia, J. J.: Aerosol composition, sources and

656 processes during wintertime in Beijing, China, *Atmospheric Chemistry and Physics*, 13, 4577–4592, 10.5194/acp-  
657 13-4577-2013, 2013.

658 Sun, Y. L., Wang, Z. F., Du, W., Zhang, Q., Wang, Q. Q., Fu, P. Q., Pan, X. L., Li, J., Jayne, J., and Worsnop, D. R.: Long-  
659 term real-time measurements of aerosol particle composition in Beijing, China: seasonal variations, meteorological  
660 effects, and source analysis, *Atmospheric Chemistry and Physics*, 15, 10149–10165, 10.5194/acp-15-10149-2015,  
661 2015.

662 Sun, Y. L., Xu, W. Q., Zhang, Q., Jiang, Q., Canonaco, F., Preevot, A. S. H., Fu, P. Q., Li, J., Jayne, J., Worsnop, D. R.,  
663 and Wang, Z. F.: Source apportionment of organic aerosol from 2-year highly time-resolved measurements by an  
664 aerosol chemical speciation monitor in Beijing, China, *Atmospheric Chemistry and Physics*, 18, 8469–8489,  
665 10.5194/acp-18-8469-2018, 2018.

666 Ulbrich, I. M., Canagaratna, M. R., Zhang, Q., Worsnop, D. R., and Jimenez, J. L.: Interpretation of organic  
667 components from Positive Matrix Factorization of aerosol mass spectrometric data, *Atmospheric Chemistry and  
668 Physics*, 9, 2891–2918, 10.5194/acp-9-2891-2009, 2009.

669 Xu, L., Suresh, S., Guo, H., Weber, R. J., and Ng, N. L.: Aerosol characterization over the southeastern United States  
670 using high-resolution aerosol mass spectrometry: spatial and seasonal variation of aerosol composition and sources  
671 with a focus on organic nitrates, *Atmos. Chem. Phys.*, 15, 7307–7336, 10.5194/acp-15-7307-2015, 2015.

672 Xu, W., Kuang, Y., Bian, Y., Liu, L., Li, F., Wang, Y., Xue, B., Luo, B., Huang, S., Yuan, B., Zhao, P., and Shao, M.: Current  
673 Challenges in Visibility Improvement in Southern China, *Environmental Science & Technology Letters*, 7, 395–401,  
674 10.1021/acs.estlett.0c00274, 2020.

675 Xu, W., Takeuchi, M., Chen, C., Qiu, Y., Xie, C., Xu, W., Ma, N., Worsnop, D. R., Ng, N. L., and Sun, Y.: Estimation of  
676 particulate organic nitrates from thermodenuder–aerosol mass spectrometer measurements in the North China  
677 Plain, *Atmos. Meas. Tech.*, 14, 3693–3705, 10.5194/amt-14-3693-2021, 2021.

678 Yang, D., Li, C., Lau, A. K. H., and Li, Y.: Long-term measurement of daytime atmospheric mixing layer height over  
679 Hong Kong, *Journal of Geophysical Research*, 118, 2422–2433, 2013.

680 Yang, S., Yuan, B., Peng, Y., Huang, S., Chen, W., Hu, W., Pei, C., Zhou, J., Parrish, D. D., Wang, W., He, X., Cheng, C.,  
681 Li, X. B., Yang, X., Song, Y., Wang, H., Qi, J., Wang, B., Wang, C., Wang, C., Wang, Z., Li, T., Zheng, E., Wang, S., Wu,  
682 C., Cai, M., Ye, C., Song, W., Cheng, P., Chen, D., Wang, X., Zhang, Z., Wang, X., Zheng, J., and Shao, M.: The  
683 formation and mitigation of nitrate pollution: comparison between urban and suburban environments, *Atmos.  
684 Chem. Phys.*, 22, 4539–4556, 10.5194/acp-22-4539-2022, 2022.

685 Yao, T., Li, Y., Gao, J., Fung, J. C. H., Wang, S., Li, Y., Chan, C. K., and Lau, A. K. H.: Source apportionment of secondary  
686 organic aerosols in the Pearl River Delta region: Contribution from the oxidation of semi-volatile and intermediate  
687 volatility primary organic aerosols, *Atmospheric Environment*, 222, 117111, 10.1016/j.atmosenv.2019.117111, 2020.

688 Yu, Y., Cheng, P., Li, H., Yang, W., Han, B., Song, W., Hu, W., Wang, X., Yuan, B., Shao, M., Huang, Z., Li, Z., Zheng, J.,  
689 Wang, H., and Yu, X.: Budget of nitrous acid (HONO) at an urban site in the fall season of Guangzhou, China, *Atmos.  
690 Chem. Phys.*, 22, 8951–8971, 10.5194/acp-22-8951-2022, 2022.

691 Zhang, Q., Jimenez, J. L., Canagaratna, M. R., Allan, J. D., Coe, H., Ulbrich, I., Alfarra, M. R., Takami, A., Middlebrook,  
692 A. M., Sun, Y. L., Dzepina, K., Dunlea, E., Docherty, K., DeCarlo, P. F., Salcedo, D., Onasch, T., Jayne, J. T., Miyoshi, T.,  
693 Shimono, A., Hatakeyama, S., Takegawa, N., Kondo, Y., Schneider, J., Drewnick, F., Borrmann, S., Weimer, S.,  
694 Demerjian, K., Williams, P., Bower, K., Bahreini, R., Cottrell, L., Griffin, R. J., Rautiainen, J., Sun, J. Y., Zhang, Y. M., and  
695 Worsnop, D. R.: Ubiquity and dominance of oxygenated species in organic aerosols in anthropogenically-influenced  
696 Northern Hemisphere midlatitudes, *Geophysical Research Letters*, 34, n/a–n/a, 10.1029/2007GL029979, 2007.

697 Zhang, Q., Jimenez, J. L., Canagaratna, M. R., Ulbrich, I. M., Ng, N. L., Worsnop, D. R., and Sun, Y.: Understanding  
698 atmospheric organic aerosols via factor analysis of aerosol mass spectrometry: a review, *Analytical and Bioanalytical  
699 Chemistry*, 401, 3045–3067, 10.1007/s00216-011-5355-y, 2011.

700 Zhang, Y. J., Tang, L. L., Wang, Z., Yu, H. X., Sun, Y. L., Liu, D., Qin, W., Canonaco, F., Prevot, A. S. H., Zhang, H. L.,  
701 and Zhou, H. C.: Insights into characteristics, sources, and evolution of submicron aerosols during harvest seasons  
702 in the Yangtze River delta region, China, *Atmospheric Chemistry and Physics*, 15, 1331-1349, 10.5194/acp-15-  
703 1331-2015, 2015.

704 Zhao, J., Qiu, Y., Zhou, W., Xu, W., Wang, J., Zhang, Y., Li, L., Xie, C., Wang, Q., Du, W., Worsnop, D. R., Canagaratna,  
705 M. R., Zhou, L., Ge, X., Fu, P., Li, J., Wang, Z., Donahue, N. M., and Sun, Y.: Organic Aerosol Processing During Winter  
706 Severe Haze Episodes in Beijing, *Journal of Geophysical Research: Atmospheres*, 124, 10248-10263,  
707 10.1029/2019JD030832, 2019.

708 Zhou, W., Xu, W., Kim, H., Zhang, Q., Fu, P., Worsnop, D. R., and Sun, Y.: A review of aerosol chemistry in Asia:  
709 insights from aerosol mass spectrometer measurements, *Environmental Science: Processes & Impacts*, 22, 1616-  
710 1653, 10.1039/D0EM00212G, 2020.

711